The Canadian Mineralogist
Vol. 47, pp. 275-296 (2009)
DOI: 10.3749/canmin.47.2.275

THE CRYSTAL CHEMISTRY OF THE KORNERUPINE–PRISMATINE SERIES. III. CHEMICAL RELATIONS

FRANK C. HAWTHORNE§ AND MARK A. COOPER

Department of Geological Sciences, University of Manitoba, Winnipeg, Manitoba R3T 2N2, Canada

EDWARD S. GREW

Department of Earth Sciences, University of Maine, Orono, Maine 04469, U.S.A.

ABSTRACT

The chemical formula of kornerupine *sensu lato* may be written as $X\ Y_2\ M_7\ T_4\ V\ O_{21}\ W$, where $X = \square$, Mg, Fe^{2+}; Y = Mg, Fe^{2+}; M = Al, Mg, Fe^{2+}, Fe^{3+}; T = Si, Al; V = Si, Al, B, Be; W = OH, F. The total number of cations is variable (14.2 to 14.4 *apfu*), the sum of the cation charge is 43+, and the amount of vacancy (*pfu*) is given by $\square = 15 - (S^{4+} + S^{3+} + S^{2+})$, where S^{Z+} is the sum of the cations of formal charge Z+. The *T*-site populations are coupled to both B and Fe^{2+} content; at moderate Si content (~3.71 Si *apfu*), the structure accommodates the largest range in B (0–0.9 *apfu*) and Fe^{2+} (0–1.3 *apfu*). Flexibility in the kornerupine structure originates at the *T*(2)–*T*(3)–*T*(2) trimer, where coupled expansion–contraction of tetrahedra and rotation [*T*(2)] proceed at the expense of sterically induced distortion of the neighboring *M*(1) and *M*(4) octahedra. Both Fe^{2+} and Mg are approximately disordered over *M*(1) and *M*(2), with the maximum $[^{M(1)}Fe^{2+} + {}^{M(2)}Fe^{2+}]$ content coupled to the B content of the crystal. The *X* site shows the greatest affinity for Fe^{2+}, with no apparent coupling of $^{X}Fe^{2+}$ to the B content. The Al contents of *M*(2) and *M*(3) + *M*(5) are strongly negatively and positively correlated, respectively, with B content. Condensing the general formula to $X\ Y_2\ M_7\ T_5\ O_{21}\ W$, the principal (heterovalent) end-member compositions for Be-free crystals are as follows:

X	***Y***	***M***	***T***		***W***
□	Mg_2	Al_5Mg_2	Si_5	O_{21}	F
□	Mg_2	Al_7	Si_3B_2	O_{21}	F
Mg	Mg_2	Al_3Mg_4	Si_5	O_{21}	F
Mg	Mg_2	Al_7	SiB_4	O_{21}	F

where Mg = $^{[8,6]}$(Mg,Fe^{2+}), Al = $^{[6]}$(Al,Fe^{3+}), Si = $^{[4]}$Si, B = $^{[4]}$(Al,B) and F = (OH,F). These compositions can be represented in the orthogonal system ^{X}Mg–^{M}Al–^{T}Si, and define a plane on which the compositions of kornerupine can be graphically represented. Chemical exchange involves the two independent substitutions: $^{X}\square + {}^{M}Al_2 = {}^{X}Mg + {}^{M}Mg_2$ and $^{M}Mg + {}^{T}Si = {}^{M}Al + {}^{T}B$. The principal homovalent chemical variations in kornerupine are $^{T}Al \rightleftharpoons {}^{T}B$ and $^{X,M}Fe^{2+} \rightleftharpoons {}^{X,M}Mg$. However, neither show a simple 1:1 substitution. For $^{T}Al \rightleftharpoons {}^{T}B$, the total amount of trivalent cations (*i.e.*, ^{T}Al + B) varies with variation in the ^{T}Al:B ratio (and hence with a change in the Si content). For $^{X,M}Fe^{2+} \rightleftharpoons {}^{X,M}Mg$, the total amount of divalent cations (*i.e.*, $^{X+M}Fe^{2+} + {}^{X+M}Mg$) varies with the variation in $^{X+M}Fe^{2+} : {}^{X+M}Mg$ ratio (and hence with a change in the ^{M}Al or $^{X}\square$ content). However, the slopes of ensuing relations are significantly less than 1.0, as these substitutions are constrained by commensurability requirements arising from the layered nature of the structure and the distribution of sites over which these substitutions act.

Keywords: kornerupine, prismatine, chemical formula, end member, chemical substitutions.

SOMMAIRE

On peut écrire la formule chimique de la kornérupine *sensu lato* $X\ Y_2\ M_7\ T_4\ V\ O_{21}\ W$, dans laquelle $X = \square$, Mg, Fe^{2+}; Y = Mg, Fe^{2+}; M = Al, Mg, Fe^{2+}, Fe^{3+}; T = Si, Al; V = Si, Al, B, Be; W = OH, F. Le nombre total de cations est variable (entre 14.2 et 14.4 *apfu*), la somme des charges positives est 43, et la proportion de lacunes par formule unitaire correspond à $\square = 15 - (S^{4+} + S^{3+} + S^{2+})$; dans cette expression, S^{Z+} représente la somme des cations de charge formelle Z+. La population des sites *T* est couplée aux teneurs de B et de Fe^{2+}; à teneur en Si modeste (~3.71 Si *apfu*), la structure peut accommoder le plus grand intervalle en bore (0–0.9 *apfu*) et en Fe^{2+} (0–1.3 *apfu*). La flexibilité de la structure de la kornérupine vient du trimère *T*(2)–*T*(3)–*T*(2), dans lequel un couplage de l'expansion ou de la contraction des tétraèdres et leur rotation [*T*(2)] procède aux dépens de la distorsion stérique induite des octaèdres *M*(1) et *M*(4) adjacents. Le Fe^{2+} et le Mg sont approximativement désordonnés sur les sites *M*(1) et *M*(2), et la teneur maximum en $[^{M(1)}Fe^{2+} + {}^{M(2)}Fe^{2+}]$ est couplée avec la teneur en bore du cristal. Le Fe^{2+} montre la plus grande affinité pour le site *X*, sans couplage apparent entre $^{X}Fe^{2+}$ et la teneur en bore. La teneur en Al des sites *M*(2) et *M*(3) + *M*(5) montre une

§ *E-mail address*: frank_hawthorne@umanitoba.ca

forte corrélation, négative et positive, respectivement, avec la teneur en bore. En condensant la formule générale à $X\ Y_2\ M_7\ T_5\ O_{21}\ W$, les compositions des pôles principaux (hétérovalents) des cristaux dépourvus de Be seraient:

X	*Y*	*M*	*T*		*W*
□	Mg_2	Al_5Mg_2	Si_5	O_{21}	F
□	Mg_2	Al_7	Si_3B_2	O_{21}	F
Mg	Mg_2	Al_3Mg_4	Si_5	O_{21}	F
Mg	Mg_2	Al_7	SiB_4	O_{21}	F

Ici, Mg = $^{[8,6]}$(Mg,Fe^{2+}), Al = $^{[6]}$(Al,Fe^{3+}), Si = $^{[4]}$Si, B = $^{[4]}$(Al,B) et F = (OH,F). On peut représenter ces compositions dans un système orthogonal ^{X}Mg–^{M}Al–^{T}Si, et définir un plan sur lequel on peut représenter graphiquement les compositions de kornérupine. L'échange chimique implique deux substitutions indépendantes: $^{X}\square + {}^{M}Al_2 = {}^{X}Mg + {}^{M}Mg_2$ et $^{M}Mg + {}^{T}Si = {}^{M}Al + {}^{T}B$. Les variations homovalentes principales dans la kornérupine sont $^{T}Al \rightleftharpoons {}^{T}B$ et $^{X,M}Fe^{2+} \rightleftharpoons {}^{X,M}Mg$. Toutefois, ni l'une ni l'autre sont des cas de simple substitution 1:1. Pour $^{T}Al \rightleftharpoons {}^{T}B$, le total des cations trivalents (*i.e.*, $^{T}Al + B$) varie avec le rapport $^{T}Al : B$ (et ainsi, avec un changement de la teneur en Si). Pour $^{X,M}Fe^{2+} \rightleftharpoons {}^{X,M}Mg$, le total des cations bivalents (*i.e.*, $^{X+M}Fe^{2+} + {}^{X+M}Mg$) varie avec la variation en $^{X+M}Fe^{2+} : {}^{X+M}Mg$ ratio (et donc avec un changement en teneur de ^{M}Al ou $^{X}\square$). Toutefois, les pentes des relations qui en résultent sont largement inférieures à 1.0 parce que ces substitutions sont régies par des exigeances de commensurabilité dues à la stratification de la structure et à la distribution des sites impliqués.

(Traduit par la Rédaction)

Mots-clés: kornérupine, prismatine, formule chimique, pôle, substitutions chimiques.

Introduction

The crystal structure of kornerupine *sensu lato* is quite complicated, with three tetrahedrally coordinated *T* sites, five octahedrally coordinated *M* sites, and one [8]-coordinated *X* site. This complexity is compounded by the fact that the three dominant cations, Mg, Al and Si, scatter X-rays in a very similar fashion, thereby making the assignment of accurate site-populations quite difficult. However, extensive work on the crystal chemistry of kornerupine (Moore & Bennett 1968, Moore & Araki 1979, Moore *et al.* 1989, Finger & Hazen 1981, Klaska & Grew 1991, Hawthorne *et al.* 1995, Cooper & Hawthorne 2009, Cooper *et al.* 2009a, b, c) has furthered considerably our knowledge of site occupancy in these minerals. In particular, Cooper *et al.* (2009a) assigned complete site-populations on the basis of X-ray site-scattering refinement, the results of electron- and ion-microprobe analysis, and variations in Fe^{3+}/Fe^{2+} ratios and H-content measured by Mössbauer spectroscopy and hydrogen-line extraction (Grew *et al.* 1990, 1999, Cooper *et al.* 2009b). These authors also considered long-range crystal-chemical relations in the kornerupine structure, particularly the systematic variation in mean bond-length as a function of the mean radius of the constituent cations.

Despite the complexity of the kornerupine structure, the kornerupine-group minerals show a surprisingly small range of chemical composition, particularly when compared to other rock-forming silicates such as pyroxene, amphibole and mica. Here, we examine chemical variations, assign end-member compositions, and examine crystal-chemical features that may constrain the variation in chemical composition of kornerupine.

The Minerals of the Kornerupine Group

Cooper *et al.* (2009a) showed that the B content of kornerupine *sensu lato* varies between 0.02 and 0.88 *apfu* (atoms per formula unit); they also showed that B is completely ordered at the *T*(3) site across the complete range of chemical variation in the kornerupine structure (Figs. 1, 2). As there is one *T*(3) site in the structural formula of kornerupine, the B content of *T*(3) can vary from 0 to 1 atoms per site. Thus there are two distinct minerals, one with B dominant (>0.5 *apfu*) at *T*(3) and the other with B subordinate to Si at *T*(3) (<0.5 *apfu*). Grew *et al.* (1996) re-introduced the name *prismatine* for the B-rich member of this series and *kornerupine* for the B-poor member. Kornerupine *sensu lato* is the group name, and kornerupine *sensu stricto* is the mineral name; a Latin modifier will be used only where ambiguity might otherwise occur.

The Chemical Formula of Kornerupine

Following normal usage for complex rock-forming silicate minerals, we wish to write the general formula of kornerupine *sensu lato* as the sum of the available occupied sites in the structure. However, there are two different ways in which this may be done. Both have their advantages (and disadvantages), and which is preferred depends on whether one is considering the crystal chemistry or the chemical composition of kornerupine. One may write the formula in the simplest way as

$$X\ M_9\ T_5\ O_{21}\ W \qquad \{1\}$$

where X = □, Mg, Fe^{2+}; M = Al, Mg, Fe^{2+}, Fe^{3+}; T = Si, Al, B, Be; W = (OH), F. The cations of the

chemical formula can be assigned to the three groups as follows:

(1) Si, B and Be are assigned to the *T* group, together with sufficient Al to bring the total number of cations to 5.00 *apfu*.

(2) The remaining Al is assigned to the *M* group, together with all Fe^{3+} and sufficient ($Mg + Fe^{2+}$) to bring the total number of cations to 9.00 *apfu*.

(3) The remaining ($Mg + Fe^{2+}$) is assigned to the *X* group.

Note that the amounts of Mg and Fe^{2+} in the *M* and *X* groups of cations cannot be determined only from the results of chemical analysis; crystal-structure refinement is required. This situation is similar to that encountered in other complex silicate minerals (*e.g.*, the cummingtonite–grunerite series and the anthophyllite–gedrite series, in which the distribution of Mg and Fe^{2+} over the *B* and *C* groups is not determined from the results of chemical analysis). The problem with representation {1} of the chemical formula is that (i) the occupancy of a specific *T* site by B (and Be) is not recognized, and (ii) the occupancy of only some of the *M* sites by Al and by Mg and Fe^{2+} is not recognized. This deficiency results in end-member compositions that are not crystal-chemically compatible with the kornerupine structure as they involve occupancy of sites that do not occur in actual compositions of kornerupine. This issue may be resolved by modifying the general formula such that the chemical species in any group are restricted in terms of their formal valence. Thus we write the general formula as

$$X\ Y_2\ M_7\ T_4\ V\ O_{21}\ W \qquad \{2\}$$

where $X = \square$, Mg, Fe^{2+} ($0, 2^+$)
Y = Mg, Fe^{2+} (2^+)
M = Al, Mg, Fe^{2+}, Fe^{3+} ($2^+, 3^+$)
T = Si, Al ($4^+, 3^+$)
V = Si, Al, B, Be ($4^+, 3^+, 2^+$)
W = OH, F (1^-)

We have specifically identified the *X* cations as occupying the [8]-coordinated *X* site, the divalent *Y* cations as occupying the [6]-coordinated *M*(1) site, the *M* cations as occupying the [6]-coordinated *M*(2–5) sites, and the *T* and *V* cations as occupying the [4]-coordinated *T*(1,2) and *T*(3) sites, respectively. As written, the cations of the chemical formula can be assigned to the five groups as follows:

(1) Be and B are assigned to the *V* group, together with sufficient (Si + Al) to bring the total to 1 *apfu*.

(2) Si is assigned to the *T* group, together with sufficient Al to bring the sum of the *T*-group cations to 4 *apfu*;

(3) the remaining Al is assigned to the *M* group, together with any other trivalent (*e.g.*, Fe^{3+}, Cr^{3+}, V^{3+}) and tetravalent (*e.g.*, Ti^{4+}) cations; the *M*-group sum is brought to 7 *apfu* by ($Mg + Fe^{2+}$);

(4) $Mg + Fe^{2+}$ = 2 *apfu* is assigned to the *Y* group;

(5) the remaining (Mg + Fe*), where Fe* = Fe^{2+} + minor Mn^{2+}, is assigned to the *X* group, together with Ca and Na.

Note that with formula {2}, we can assign only (Si + Al) to the *T* and *V* sites, and not specific amounts of Si and Al. Moreover, as with formula {1}, we can assign only ($Mg + Fe^{2+}$) to the *M* and *X* sites, and not specific amounts of Mg and Fe^{2+}. However, with formula {2}, we can write end-member compositions that are crystal-chemically realistic and represent real variations in the chemical composition of kornerupine. By analogy with other complex minerals (*e.g.*, amphiboles), one might expect any Mn^{2+} to show a preference for the *X* group.

Major- and Minor-Element Variations in Kornerupine

The compositional ranges observed by Cooper *et al.* (2009a) are listed in Table 1, and the corresponding variations in site populations are given in Table 2. Their sampling of kornerupine from different localities is fairly extensive, and hence the ranges given in Table 1 should be fairly representative of natural compositions. Obviously, these chemical ranges are not independent of each other, as overall electroneutrality must be maintained, and they may be further affected by local crystal-chemical factors such as bond-valence requirements or steric restrictions. To a reasonable approximation, the (*T* + *V*)-group cations and the (*M* + *Y*)-group cations are each a ternary system. Compositional variation for the crystals refined here are shown in Figure 3. For the (*T* + *V*)-group cations (Fig. 3a), B increases from 0.0 to 0.9 *apfu* with minor increase in Si (from 3.5 to 3.9 *apfu*) and large decrease in Al (from 1.5 to 0.2 *apfu*). For the (*M* + *Y*)-group cations (Fig. 3b), Fe^{2+} increases from 0 to 1.3 *apfu*, with a minor increase in Al* (from 5.4 to 5.9 *apfu*; Al* = Al + Fe^{3+} + Ti^{4+} +V^{3+} + Cr^{3+}) and a major decrease in Mg (from 3.8 to 2.0 *apfu*).

TABLE 1. KORNERUPINE: RANGES IN OXIDE AND ION CONTENTS*

Oxide	wt.%			Ion	*apfu*		
SiO_2	28.53	–	32.38	Si	3.55	–	3.88
Al_2O_3	37.75	–	49.57	Al	5.60	–	7.16
B_2O_3	0.08	–	4.21	B	0.02	–	0.88
MgO	10.81	–	21.74	Mg	2.06	–	3.92
FeO	0	–	12.09	Fe^{2+}	0	–	1.29
Fe_2O_3	0	–	3.63	Fe^{3+}	0	–	0.35
MnO	0	–	0.35	Mn^{2+}	0	–	0.04
V_2O_3	0	–	0.20	V^{3+}	0	–	0.02
Cr_2O_3	0	–	0.28	Cr^{3+}	0	–	0.03
TiO_2	0	–	0.30	Ti^{4+}	0	–	0.03
Na_2O	0	–	0.14	Na	0	–	0.03
CaO	0	–	0.09	Ca	0	–	0.01
F	0	–	0.94	F	0	–	0.37
H_2O	0.75	–	1.23	H	0.63	–	1.00
				Cation sum	14.18	–	14.41
				□	0.82	–	0.59

*Data from Cooper *et al.* (2009a).

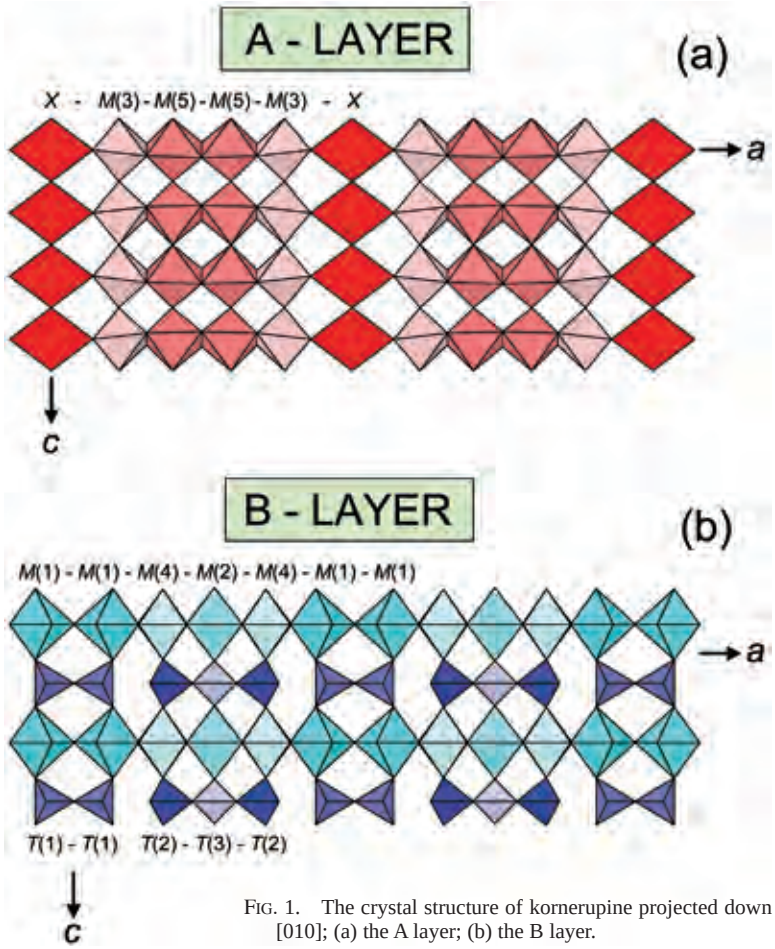

FIG. 1. The crystal structure of kornerupine projected down [010]; (a) the A layer; (b) the B layer.

VARIATION IN AGGREGATE-CATION CHARGE AT THE *X*, *(Y + M)* AND *T* SITES

Variation in $^{X}\square$

The amount of vacancy in any kornerupine is controlled by the amount and charge of its constituent cations and the requirement that the structure be electronically neutral. However, electron-microprobe analysis does not provide a complete measure of the amount of trivalent cations (*i.e.*, B and Fe^{3+} are not determined). Site-scattering results from structure refinement are essential in determining the correct numbers of differently charged species and the correct number of total cations (including the □ content). Where these values are known, the □ content of the *X* site is

$$\square = 15 - S^{4+} - S^{3+} - S^{2+} \quad (1)$$

where S^{Z+} is the sum of the cations of formal charge Z+.

TABLE 2. TOTAL VARIATION IN SITE POPULATIONS (*apfu*) IN KORNERUPINE CRYSTALS OF COOPER *et al.* (2009a)

T(1)	Si: 1.800–2.000	Al: 0.000–0.200	
T(2)	Si: 1.016–1.798	Al: 0.202–0.984	
T(3)	Si: 0.057–0.727	Al: 0.053–0.299	B: 0.016–0.880
M(1)	Mg: 1.292–1.988	Fe^{2+}: 0.012–0.708	
M(2)	Mg: 0.448–0.909	Al: 0.062–0.189	Fe^{2+}: 0.000–0.466
M(3)	Al: 1.884–1.990	Mg: 0.010–0.116	
M(4)	Al: 1.142–1.780	Mg: 0.192–0.630	Fe^{3+}: 0.000–0.348
M(5)	Al: 1.920–1.988	Mg: 0.012–0.080	
X	Mg: 0.073–0.393	Fe^{2+}: 0.000–0.231	□: 0.597–0.815

Cooper *et al.* (2009b) showed that the sum of (OH) + F is invariably 1.0 *apfu* in kornerupine. The *T*, *V*, *Y* and *M* sites contain 14 cations *pfu* $[T(1)_2 + T(2)_2 + T(3)_1 + M(1)_2 + M(2)_1 + M(3)_2 + M(4)_2 + M(5)_2]$, and the *X* site, primarily occupied by □, contains Mg + Fe* from 0.18 to 0.41 cations *pfu*. As a result, there is a variable

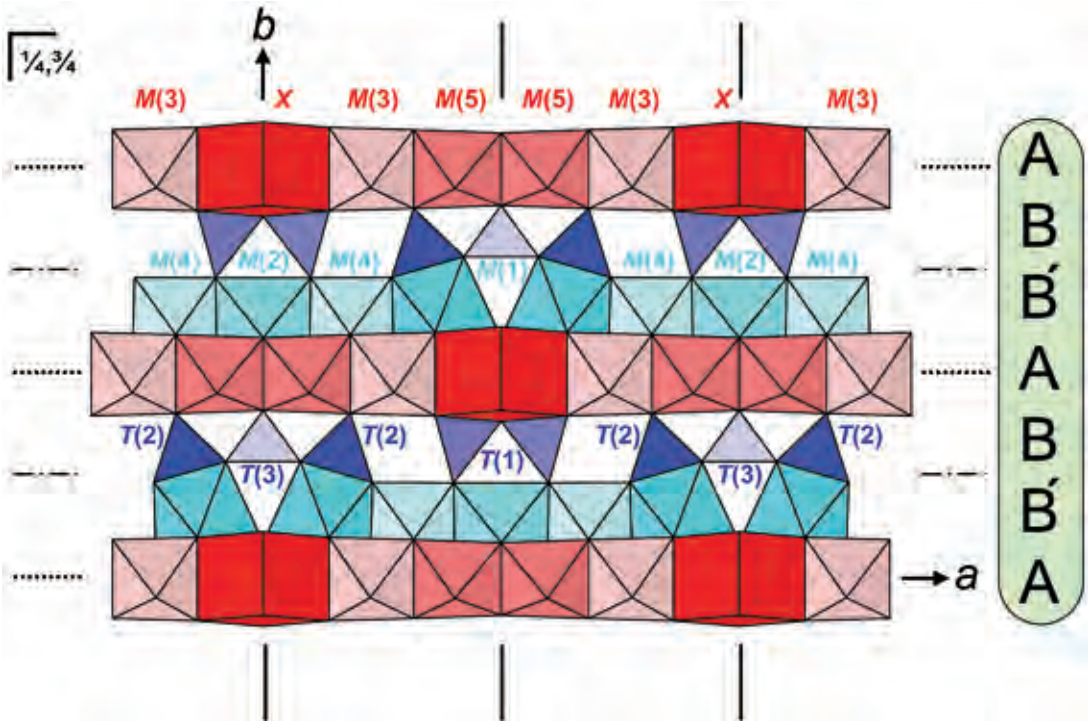

FIG. 2. The crystal structure of kornerupine projected down [001] with the A and B layers shown.

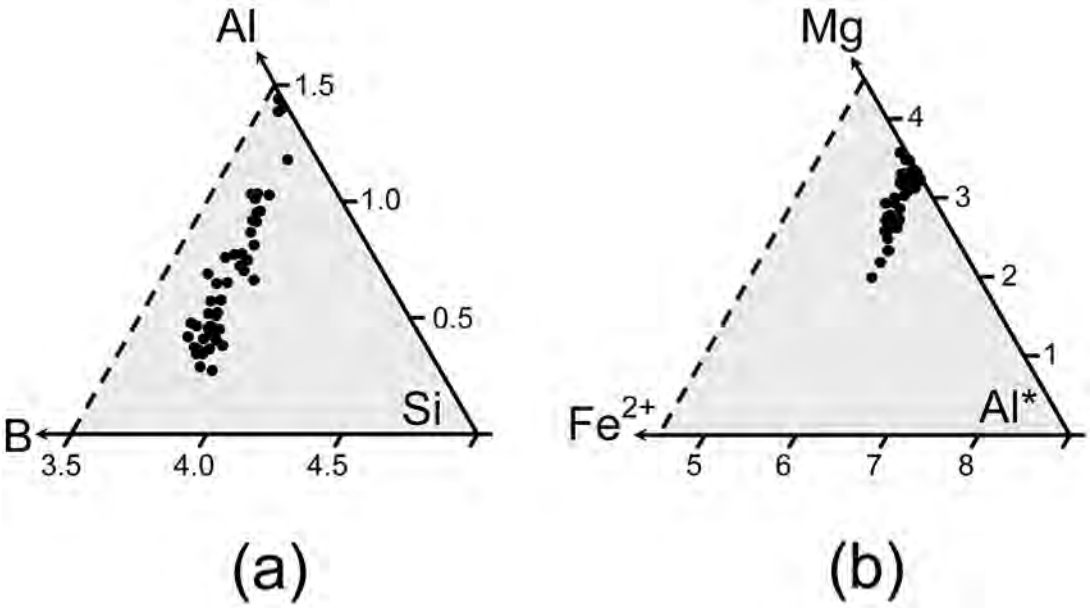

FIG. 3. Chemical variation in kornerupine *sensu lato*: (a) B *versus* Al *versus* Si within the (*T* + *V*) group (5 *apfu*); (b) Mg *versus* Fe *versus* Al* within the (*M* + *Y*) group (9 *apfu*). Here, Al* = Al + (Fe^{3+}, Ti^{4+}, V^{3+}, Cr^{3+}); data from Cooper *et al*. (2009a).

number of cations, the charges of which must sum to 43^+ *pfu*. To maintain this overall cation-charge, the variable content of cations (and therefore vacancy content) of the *X* site is coupled to changes in the proportion of divalent : trivalent : tetravalent cations in the rest of the structure; this relation is shown in Figure 4. In Figure 4a, the sum of the divalent cations in the structure is plotted against the sum of the tetravalent cations. Variation in the amount of tetravalent cations corresponds to variation in Si, as Ti^{4+} is the only other tetravalent cation present, and it occurs only in very minor amounts (<0.03 *apfu*). The divalent-cation total reflects the sum (Mg + Fe + Mn) (as Ca values are insignificant). The trivalent-cation total (Al + B + Fe + Cr + V + [Ti^{4+}]) is plotted against the tetravalent-cation total (Si) in Figure 4b. Parallel dashed lines represent contours of constant $^X\square$ (vacancy). Substitutions involving adjustments to divalent–trivalent cation ratios with changing Si can be quite variable. If the substitution occurs with no change in cation total, then the substitution must parallel the dashed lines [*i.e.*, a Tschermak-type substitution: $^{[6]}3^+ + {}^{[4]}3^+ \rightleftharpoons {}^{[6],[8]}2^+ + {}^{[4]}4^+$. All substitutions that are not parallel to the dashed lines involve an additional coupled substitution with $^X\square$. The distribution of data in Figure 4 shows that the lowest and highest Si values occur at ~0.67 $\square$ [the highest and lowest 4^+ cation totals occur at $^X\square \approx 0.67$]. Thus over the maximum range in Si, the Tschermak-type substitution is able to accommodate changes in 2^+, 3^+ and 4^+ cations without necessarily involving a $\square$ substitution. With increasing $\square$ (*i.e.*, 0.67 $\square \rightarrow$ 0.82 $\square$), the observed range of the Tschermak-type substitution decreases, extrapolating to zero at $\square \approx 0.88$ *pfu*. In summary, the Tschermak-type substitution is potentially most extensive at relatively low $\square$, and substitutions involving $\square$ at the *X* site are most extensive at intermediate Si content.

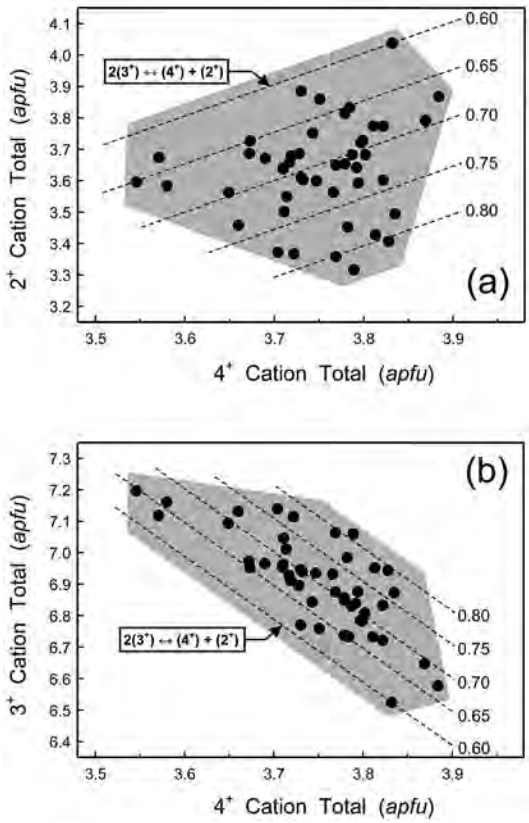

FIG. 4. Chemical variation in kornerupine *sensu lato*: (a) divalent cation total (Mg + Fe + Mn) *apfu versus* the tetravalent cation total (Si) *apfu*; (b) trivalent cation total [Al + B + Fe + Cr + V + (Ti^{4+})] *versus* the tetravalent cation total (Si). Dashed lines are contours representing constant $\square$ *pfu*.

CRYSTAL CHEMISTRY OF THE *T* SITES

The *T*(1), *T*(2) and *T*(3) tetrahedra polymerize to form two distinct clusters, a [T_2O_7] dimer and a [T_3O_{10}] trimer, both of which occur within the B layer of the structure (Figs. 1b, 2). Cooper *et al.* (2009a) show that B occurs only at the *T*(3) site, whereas Si and Al occur at the *T*(1), *T*(2) and *T*(3) sites.

Si, Al order

Figure 5a shows the relative partitioning of Si over *T*(1), *T*(2) and *T*(3) with increasing Si. About half the Si present occurs at the *T*(1) site, the other half being partitioned between *T*(2) and *T*(3) in an increasingly disproportionate manner with increasing Si. Maximal variability of Si occurs at moderate Si content (~3.7 *apfu*), whereas at very low and very high Si contents, the distribution of Si over the *T* sites is constrained within narrow limits. The total Si content of kornerupine is shown as a function of B content in Figure 5b; there is a broad positive correlation, the data occupying a shaded parallelogram. At extreme Si values, the B content is constrained within narrow limits, whereas at moderate Si content (~3.7 *apfu*), the largest range in B content occurs. Order of Si and Al at the *T*(1), *T*(2) and *T*(3) sites is shown in Figure 5c. For all *T*-site compositions, the *T*(1) site shows the greatest affinity for Si relative to Al, with a maximum of 10% Al present at *T*(1). The degree of order of (Si, Al) at *T*(2) and *T*(3) is more variable for a given Si value. A transition region occurs at moderate Si content, where Si and Al are more or less disordered over the *T*(2) and *T*(3) sites. At lower Si values, Si prefers *T*(3) over *T*(2), and at higher Si values, the situation is reversed. The Si content of *T*(1), *T*(2) and *T*(3), and the Al content of *T*(3), are shown as a function of B content in Figure 6. The variation in Si and Al at all *T* sites is systematic with regard to increasing B at *T*(3). Line segments drawn through the

data indicate a constant variation in Si → Al at *T*(1), and a possibly different behavior in Si ⇌ Al substitution at low B values (*i.e.*, B < ~0.2 *apfu*) as compared to higher B values for the *T*(2) and *T*(3) sites.

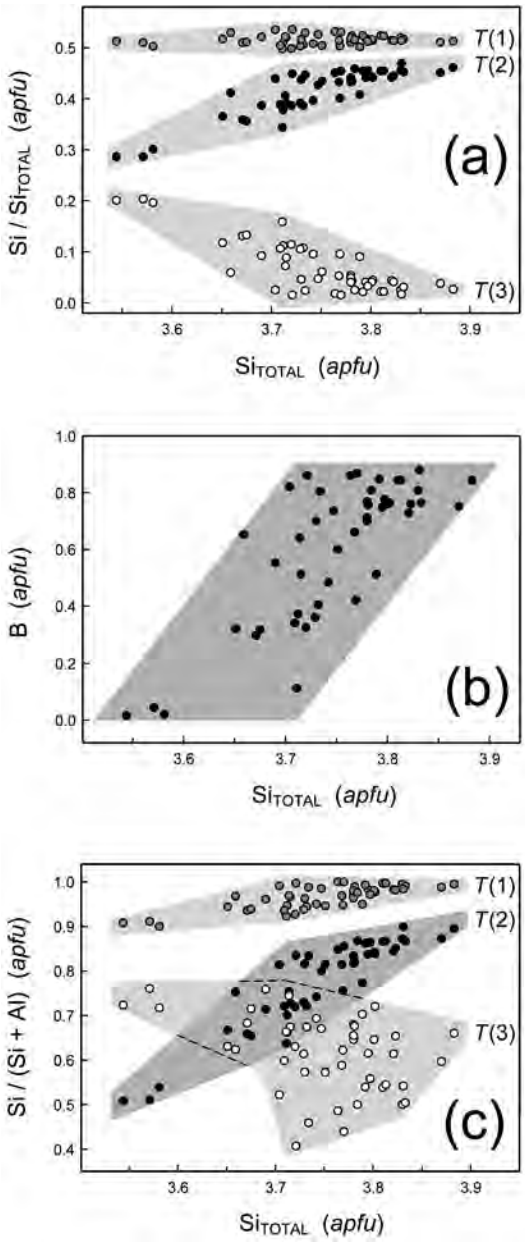

FIG. 5. The *T*-site composition in kornerupine: (a) relative Si content of the *T* sites *versus* total Si content; (b) B content *versus* Si content; (c) Si / (Si + Al) distribution for the *T* sites *versus* total Si.

The B content at *T*(3) correlates well with specific (Si, Al) distributions at all three tetrahedra. The relations in Figure 6 clearly indicate the following aggregate coupled substitution at the *T* sites:

$$^{T(1)}Si_{0.2} + {}^{T(2)}Si_{0.8} + {}^{T(3)}B_{0.7}(Al) \rightleftharpoons {}^{T(1)}Al_{0.2} + {}^{T(2)}Al_{0.8} + {}^{T(3)}Si_{0.7} \quad (2)$$

This equation does not take into account the break in slope at B = 0.20 *apfu* in Figure 6, but any inaccuracy thereby introduced is very minor. Note that this net chemical exchange does not conserve charge and hence must couple to heterovalent substitutions in other parts of the structure.

The T(3) site

The variation in composition of the *T*(3) site is shown in Figure 7. The data follow closely the line 4B ⇌ 3Si + Al (but shifted ~0.04 toward the Al apex of the composition triangle), indicating strong coupling among the Si, Al and B occupancies of *T*(3).

T-site occupancies and Fe^{2+} and Fe^{3+} contents

The Si composition is plotted against the Fe* content [Fe* = Fe^{2+} + Mn^{2+}] in Figure 8. The data lie within the confines of the shaded triangle, and the apex of the triangle is located near 1.5 Fe* and 3.7 Si *apfu*. The most Fe-rich sample from Cooper *et al.* (2009a) (shown in Fig. 8) contains 1.31 Fe* *apfu*, whereas the maximum total Fe content reported overall is 15 wt.% Fe as FeO; *i.e.*, ~1.6 Fe *apfu* (Wanni Complex, Sri Lanka, Grew *et al.* 1995). Color and compositions of associated minerals suggest that some of the Fe is ferric in the Sri Lanka sample, but the Massif Central sample is colorless, and its Fe^{3+} content is probably negligible. The well-defined convergence of data near the apex

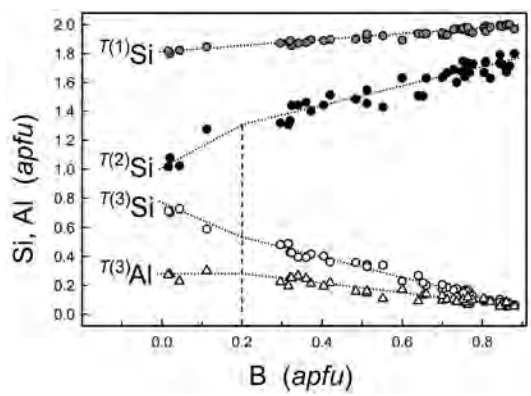

FIG. 6. Variation in selected *T*-site populations as a function of B content in kornerupine.

of the shaded area in Figure 8 suggests a maximum possible Fe* content in kornerupine of about 1.5 Fe* *apfu*, which is only 0.1 Fe *apfu* less than the Fe content of the Massif Central kornerupine. Thus Fe^{2+} = 1.6 *apfu* could be the maximum possible; this kornerupine has reacted to form sekaninaite, the Fe-dominant analogue of cordierite; *i.e.*, a composition close to the maximum Fe^{2+} content in cordierite-group minerals.

In Figure 8, the shading of the data points according to the B content of the crystal shows that high B (*i.e.*, 0.67–1.0 B *apfu*) *and* moderate Si (~3.7 Si *apfu*) are required for maximal incorporation of Fe*. The *T*-site compositions are shown as functions of Fe* content in Figure 9. It is apparent that variability of occupancy at the *T* sites is strongly related to Fe^{2+} content. A fully Si-occupied *T*(1) site (*i.e.*, 2 Si *apfu*), combined with a relatively high Si content (~1.7 Si *apfu*) at *T*(2) and high B content at *T*(3), correlates with high Fe* content. Note that similar *T*-site compositions also occur for Fe*-poor kornerupine. From the positions of the leading edges of the shaded data-fields in Figure 9, it is apparent that 0 → 0.4 Fe* *apfu* can freely enter the kornerupine structure at any *T*-site composition, and that above 0.4 Fe* *apfu*, the variability of the *T*-site populations is increasingly more restricted with increasing Fe* content.

At moderate Si compositions (Si ~ 3.7 *apfu*), the kornerupine structure is at its most flexible, showing the greatest range in *T*-site populations (Fig. 5c), and the largest ranges in B and Fe* contents (Figs. 5b, 8). Figures 5, 6, 7 and 9 show a complex interplay of (Si ⇌ Al) substitution over the three *T*-sites, an interplay that is tied to the B content at *T*(3) and that governs the maximum content of Fe^{2+} at the *X* and *M* sites. Structural relaxation associated with increasing B at *T*(3) [and complementary (Si, Al) order at *T*(1) and *T*(2)] is the most important factor associated with increasing Fe^{2+} → Mg substitution. Reduction in size of the *T*(3) (B → Si, Al) and *T*(2) (Si → Al) tetrahedra and rotation of the *T*(2) tetrahedron (Fig. 10) produce a geometrical relaxation that is conducive to Fe^{2+} → Mg substitution at *M*(1) and *M*(2).

A maximum limit on the Fe content of kornerupine*

From their study of an Fe-rich kornerupine (12.2 wt.% FeO), Finger & Hazen (1981) concluded that there are no obvious structural limitations on Fe^{2+} → Mg substitution in kornerupine. The convergence of the data in Figure 8 (near the apex at ~1.5 Fe* *apfu*) indicates otherwise. The Fe* content is plotted against B content in Figure 11; the heavy-dashed line marks the upper extent of the data. There is an obvious relation between the upper limit of Fe* content and the B content. In these crystals, the *X* site is occupied by minor Mg or ($Mg + Fe^{2+}$) and substantial vacancy. At the *X* site, Fe* / (Fe* + Mg) ranges from 0 to 0.76 for the crystals studied here. With no obvious stereochemical basis on which to restrict access by Fe^{2+}, perhaps availability of Fe^{2+} is the main factor controlling Fe^{2+} occupancy of the *X* site. The heavy-dashed line in Figure 11 may therefore not provide the best estimate of the upper limit of Fe* incorporation into the kornerupine structure. As such, we have raised the upper limit in Figure 11 by replotting the data points (white circle) with *adjusted* Fe* values that include all observed ^{X}Mg "converted" to ^{X}Fe. The new upper limit is marked with a thin-dashed line, and this thin-dashed line may be a more accurate structural limit on mutually dependent Fe* and B incorporation in

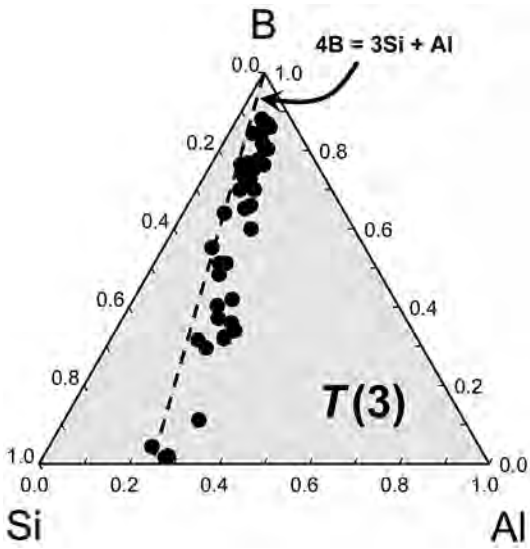

FIG. 7. Variation in site populations at the *T*(3) site in kornerupine.

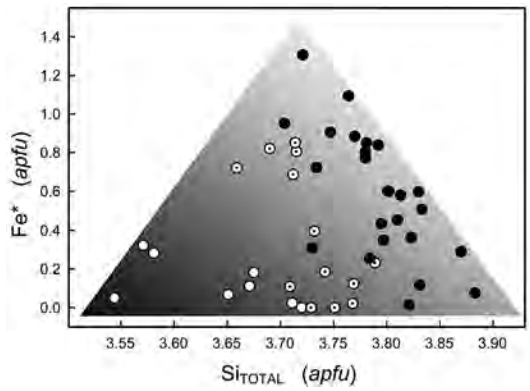

FIG. 8. Variation in Fe* (= Fe^{2+} + Mn^{2+}) as a function of total Si content in kornerupine; white circles: 0.00 < B < 0.33 *apfu*; dotted circles: 0.33 < B < 0.67 *apfu*; black circles: 0.67 < B < 1.00 *apfu*.

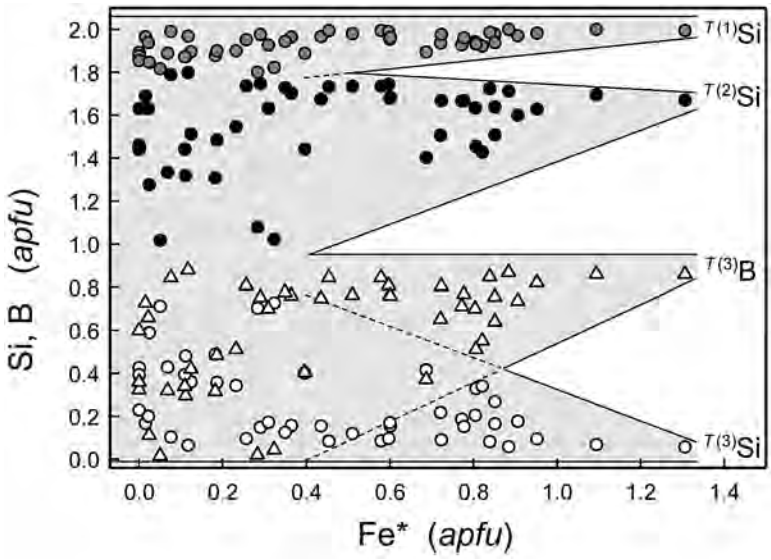

FIG. 9. Variation in Si and B *T*-site populations as a function of Fe* (= Fe^{2+} + Mn^{2+}) content in kornerupine.

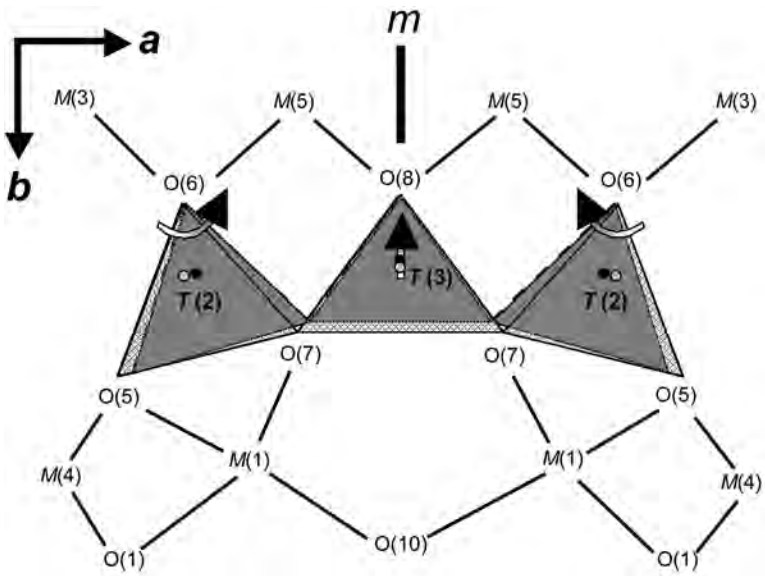

FIG. 10. The *T*(2)–*T*(3)–*T*(2) trimer of tetrahedra and neighboring environment in kornerupine, projected down [001]. Two extreme compositions are shown; K35 (low B), tetrahedra are shaded light grey, *T* sites are light grey circles; K41 (high B) tetrahedra are shaded dark grey, *T* sites are black circles.

kornerupine (note that the maximum Fe* content at the maximum possible value of B, 1 *apfu*, is 1.55 Fe* *apfu*). Where a particular data-point in Figure 11 falls short of the allowed structural limit for Fe* incorporation, is this indicative of a lack of available Fe^{2+} in the rock, or does it indicate that Fe^{2+} preferred one or more of the coexisting phases? Grew *et al.* (1990) showed that as the B content of kornerupine increases, Fe^{2+} / (Mg + Fe^{2+}) decreases relative to the values in coexisting minerals. Thus even though the structure may be able to accommodate a larger amount of Fe at higher B values (Figs. 8, 9, 11), high-B kornerupine is a less effective host for Fe compared to other coexisting phases, resulting in the scatter of data points at high B values (Fig. 11). For kornerupine of lower B content, the situation is more straightforward; the data points falling well below the structural limit in Figure 11 are clearly indicative of Fe-poor environments.

Crystal Chemistry of the *M* and *X* Sites

Fe–Mg order at X, M(1) and M(2)

A comparison of the Fe^{2+} content at the *M*(1), *M*(2) and *X* sites is shown in Figure 12a. The Fe^{2+} content at *M*(1) is approximately twice that at *M*(2), indicating that the preference of Fe^{2+} for these two sites is very similar [*i.e.*, the site multiplicity of *M*(1) is twice that of *M*(2)]. The Fe^{2+} content of the *X* site is more variable, but does not exceed ~0.2 *apfu*. The degree of order of Fe^{2+} and Mg over the *M*(1), *M*(2) and *X* sites is compared in Figure 12b. The *M*(1) and *M*(2) data overlap completely, indicating a similar distribution of Fe^{2+} and Mg over these two sites (with respect to total Fe^{2+}). The large field of data corresponds to the

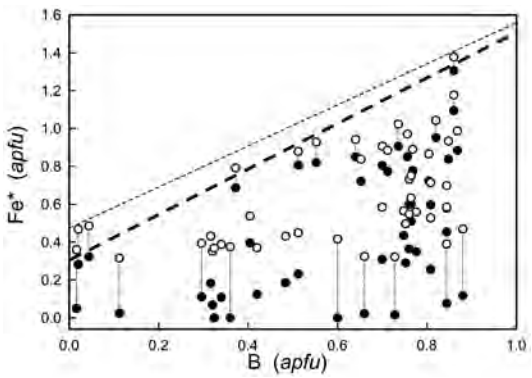

FIG. 11. Variation in Fe* (≡ Fe^{2+} + Mn^{2+}) as a function of B content in kornerupine. Black circles: observed values for Fe* and B; white circles: the value of Fe* has been adjusted by converting all Mg at *X* to Fe*; the dashed lines show the upper extent of each set of values. Several adjusted pairings are indicated with the vertical dotted lines.

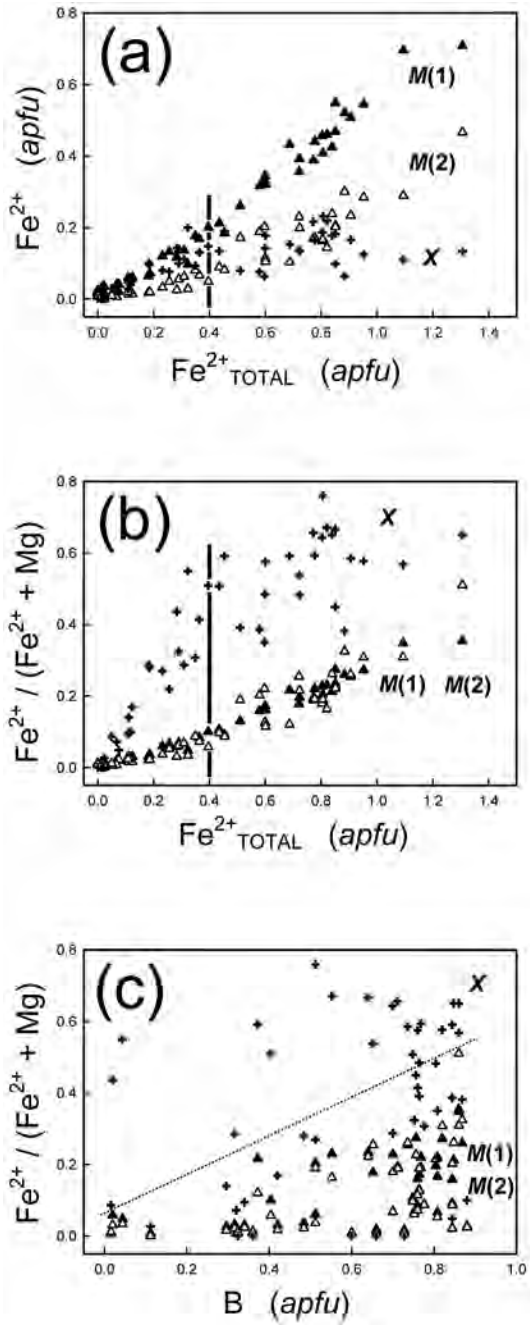

FIG. 12. The behavior of Fe^{2+} at the *X*, *M*(1), and *M*(2) sites in kornerupine: (a) variation in Fe^{2+} as a function of total Fe^{2+} content; (b) variation in Fe^{2+} / (Fe^{2+} + Mg) as a function of total Fe^{2+} content; (c) variation in Fe^{2+} / (Fe^{2+} + Mg) as a function of B content. Crosses: *X* site; black triangles: *M*(1) site; white triangles: *M*(2) site.

X site and lies appreciably above the *M*(1)–*M*(2) data, suggesting that the *X* site invariably has the greatest affinity for Fe^{2+} (relative to Mg). Figures 12a and 12b indicate a change in uptake of Fe^{2+} and the degree of (Fe^{2+}, Mg) order at about 0.4 *apfu* Fe^{2+}. These subtle changes result from direct coupling of the tetrahedra to the *M*(1) and *M*(2) sites (*cf.* Fig. 2). The degree of order of Fe^{2+} and Mg over the *M*(1), *M*(2) and *X* sites as a function of the B content is shown in Figure 12c. For a given B content, there is no restriction on (Fe, Mg) order at *X*. The maximum $Fe^{2+} \rightarrow$ Mg substitution at the *M*(1) and *M*(2) sites is coupled to the overall B content (dotted line, Fig. 12c).

Al order at the M(2), M(3), M(4) and M(5) sites

There is a well-defined inverse linear relation between $^{M(2)}$Al and $^{T(3)}$B (Fig. 13a). At high values of B, the *M*(2) site is dominated by (Mg + Fe^{2+}), and the Fe^{2+} occupancy may reach ~50% (Table 2). Examination of the B layer (Fig. 1b) shows that one repeat distance along *c* involves an *M*(2) octahedron and a *T*(3) tetrahedron that share corners through the O(8) anion. With a high B content at *T*(3), one might anticipate a short *c* cell-dimension. However, over the entire range of B content, the range in the *c* cell-dimension is only 0.07 Å (6.69–6.76 Å; Cooper *et al.* 2009a, Table 3). The O(8)–O(8) edge of the *T*(3) tetrahedron is parallel to [001] and varies in length from 2.73 to 2.51 Å with increasing B. This value is much greater than the variation in *c*, and a large component of the shortening along the O(8)–O(8) edge is compensated by a corresponding lengthening of the *M*(2) octahedron along [001]. This lengthening of the *M*(2) octahedron is accompanied by the incorporation of cations of increased radius [*i.e.*, (Mg + Fe^{2+}) → Al] at the *M*(2) site.

Figure 13b shows [$^{M(3)}$Al + $^{M(5)}$Al] as a function of B content. There is a reasonable positive correlation between Al and B. The variation in Al population is coupled to ~5% substitution by Mg. The wall of edge-sharing and corner-sharing *M*(3) and *M*(5) octahedra in the A layer (Fig. 1a) must match the dimensional changes occurring in the adjacent B layer (Figs. 1b, 2) with changing B content. At high B content, the B layer (Fig. 1b) will be somewhat shortened along *a* and *c*. Matching of the A layer to this shortened B layer requires that *M*(3) and *M*(5) contain smaller cations (dominantly Al). At low B content, the B layer expands along *a* and *c*, and the A layer adjusts *via* Mg → Al substitution.

Figure 13c shows the trivalent-cation (Al + Fe^{3+} + Cr + V + [Ti^{4+}]) content at *M*(4) *pfu* as a function of B content [the $^{M(4)}$Mg content is that which brings the *M*(4) cation-sum to 2 *apfu*]. At very low B content, the M^{3+}/ M^{2+} ratio at *M*(4) seems invariant. With increasing B content, the M^{3+}-cation content at *M*(4) may increase slightly, decrease appreciably (up to 0.4 *pfu* Mg → 3^{+}), or adjust somewhere between these extremes. The *M*(4) site is occupied primarily by Al, but also contains up to ~0.35 Fe^{3+} and ~0.63 Mg *pfu* (Table 3). The <*M*(4)–O> distances span less than 0.04 Å (Cooper *et al.* 2009a, Table 6) and the <*M*(4)–O> *versus* <$r^{M(4)}$> relation (Cooper *et al.* 2009a, Fig. 8c) has a shallow slope (0.78). Within the B layer (Fig. 1b), *M*(4) occurs between *M*(1) and *M*(2), and shares edges with both *M*(1) and *M*(2). Variable $Fe^{2+} \rightarrow$ Mg substitution at *M*(1) and *M*(2) will thus perturb the *M*(4) octahedron. All of these factors complicate understanding the role

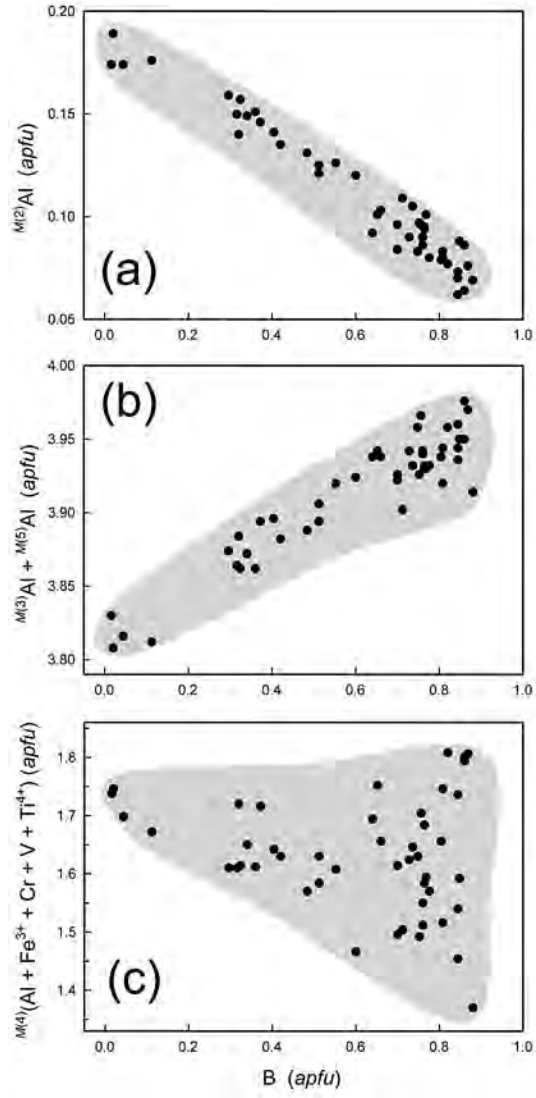

FIG. 13. Variation in trivalent *M*-cation site-populations as a function of B content in kornerupine: (a) $^{M(2)}$Al; (b) $^{M(3)}$Al + $^{M(5)}$Al; (c) $^{M(4)}$(Al + Fe^{3+} + Cr^{3+} + V^{3+} + Ti^{4+}).

of the *M*(4) octahedron in the crystal chemistry of kornerupine. The fact that the M^{3+}:M^{2+} ratio at *M*(4) can either remain invariant, or change significantly, suggests that substitution at *M*(4) may be coupled to Tschermak-type substitutions in the rest of the structure, in addition to those involving □. There is a crude correlation between the M^{3+}-cation content at *M*(4) and □ at *X* (Fig. 14a). The dashed line has a slope of 2 and represents the substitution:

$$^{M(4)}M^{3+}{}_2 + {}^{X}\square \rightleftharpoons {}^{M(4)}M^{2+}{}_2 + {}^{X}M^{2+} \quad (3)$$

Deviations from this relation in Figure 14a (broken line) may be caused by a Tschermak-type substitution that involves the *M*(4) site. Multiple-regression analysis using □ and Si *pfu* as independent variables gives an improved relation ($r^2 = 0.97$) for the $^{M(4)}M^{3+}$ content. Figure 14b compares the corresponding observed and calculated trivalent-cation contents at the *M*(4) site. The $M^{2+} \rightleftharpoons M^{3+}$ substitutions occurring at *M*(4) therefore buffer the geometrical changes that occur with varying B and $Fe^{2+} \rightleftharpoons$ Mg substitution, as well as charge differences associated with Tschermak-type and □-type substitutions.

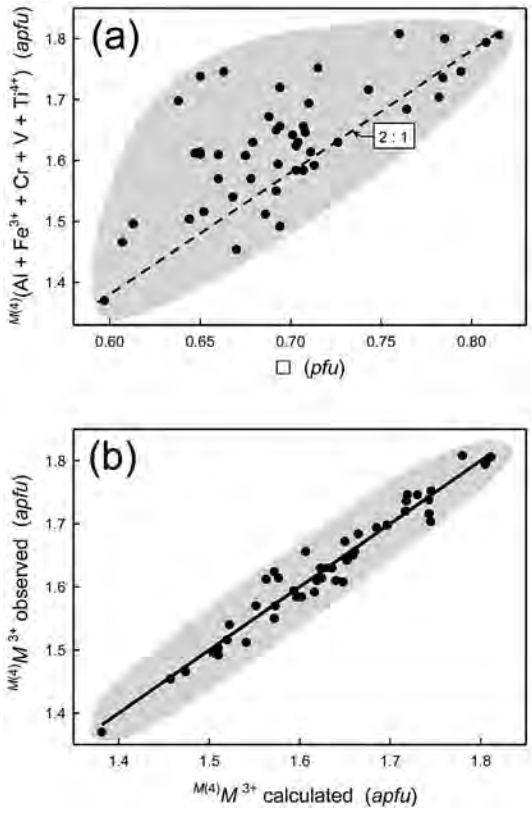

FIG. 14. The trivalent-cation content at the *M*(4) site in kornerupine: (a) variation in $^{M(4)}$(Al + Fe^{3+} + Cr^{3+} + V^{3+} + Ti^{4+}) as a function of □ content; the broken line has a slope of 2, and represents substitution $^{M(4)}M^{3+}{}_2 + {}^{X}\square \rightleftharpoons {}^{M(4)}M^{2+}{}_2 + {}^{X}M^{2+}$; (b) observed and calculated values of $^{M(4)}M^{3+}$ (calculated from the regression equation $^{M(4)}M^{3+}$ = 4.01(2) + 1.77(5)□ – 0.97(4)Si.

KORNERUPINE: ROOT COMPOSITION AND END MEMBERS

The general formula of kornerupine may be simplified to an arrangement of charges over the structure by ignoring all homovalent substitutions and writing the formula in terms of one species for each formal valence and coordination number: $^{[4]}4^{+}$ = Si, $^{[6]}3^{+}$ = Al, $^{[4]}3^{+}$ = B, $^{[6],[8]}2^{+}$ = Mg, $^{[4]}2^{+}$ = Be, 1^{-} = F, 0 = □ (vacancy):

$$(\square, Mg)\ Mg_2\ (Al,Mg)_7$$
$$(Si,B)_4\ (Si,B,Be)\ O_{21}\ F \quad \{3\}$$

We have written the *W* anion as F because this avoids complications related to the fact that the *X* site can only be (long-range) half occupied where *W* = (OH), due to the mutual interference between the *X* cation and the H atom where both are locally occupied. This complication does not arise where *W* is occupied by F (the H site is vacant) and the occupancy of the *X* cation is not constrained in this fashion.

Principal end-members

End-member compositions must show the maximum possible order for the specific arrangement of charges in the structure. Thus only one group (*i.e.*, site or group of sites) can have more than one (*i.e.*, two) constituents (Hawthorne 2002). For the formula *X* Y_2 M_7 T_4 *V* O_{21} *W*, we may use a single species for each formal valence and coordination number, and write

X	$^{[8]}$Mg (≡ Mg + Fe^{2+})
	$^{[8]}$□
Y = *M*(1)	$^{[6]}$Mg (≡ Mg + Fe^{2+})
M = *M*(2)–*M*(5)	$^{[6]}$Al (≡ Al + Fe^{3+} + Cr^{3+} + V^{3+})
	$^{[6]}$Mg (≡ Mg + Fe^{2+})
T = *T*(1)–*T*(2)	$^{[4]}$Si
	$^{[4]}$B (≡ Al)
V = *T*(3)	$^{[4]}$Si
	$^{[4]}$B (≡ B + Al)
	$^{[4]}$Be
W = O(10)	F (≡ OH + F)

Note that B here refers to all $^{[4]}3^{+}$ species, including $^{[4]}$B and $^{[4]}$Al , and that the *actual* B content cannot exceed 1 *apfu*. Moreover, we write *W* as F because *W* is not occupied by (OH) where *X* is occupied by Mg owing to the close proximity of ^{X}Mg and H. The simplified general formula may thus be written as:

$$^{X}(\square,Mg)\ ^{M(1)}Mg_2\ ^{M(2-5)}(Al,Mg)_7\ ^{T(1,2)}(Si,B)_4\ ^{T(3)}(Si,B,Be)\ O_{21}\ ^{W}F \quad \{4\}$$

For this formula, all distinct heterovalent end-members (Hawthorne 2002) are listed in Table 3; all homovalent end-members can be derived by substitutions of the type

$Fe^{2+} \rightarrow Mg$ at *X*, *M*(1) and *M*(2)

$Fe^{3+} \rightarrow Al$ at *M*(4)

$OH \rightarrow F$ at *W*

We suggest that compositions with ^{X}Fe or $^{M(1)}$Fe dominant are unlikely to occur for reasons discussed above. Within the *M* group of cations occupying the *M*(2–5) sites (Figs. 1, 2), Fe^{2+} may become dominant at the *M*(2) site. Thus in crystal K11 of Cooper *et al.* (2009a), *M*(2) is occupied by 0.466 Fe^{2+} + 0.448 Mg + 0.086 Al, indicating that this composition could be identified as a new species with Fe^{2+} dominant at *M*(2). However, taking this route would involve separately identifying the *M*(2) site (plus other sites) in the formula of kornerupine. This approach would make naming of a specific composition impossible without crystal-structure refinement, not a very useful restriction for the nomenclature scheme of a mineral series. Hence we choose to treat the *M*(2–5) sites together as containing the *M*-group cations. In principle, one could make the same argument against identifying the cations at the *M*(1) site as the *Y*-group cations. However, as noted above, Fe^{2+} is extremely unlikely to be the dominant *M*(1) (and hence *Y*-group) cation, and hence the exact *M*(1) site-populations are not necessary for naming the mineral.

Of the principal heterovalent end-members in Table 3, we can take composition (1) $^{X}\square\ ^{M(1)}Mg_2\ ^{M(2-5)}(Al_5Mg_2)\ ^{T(1,2)}Si_4\ ^{T(3)}Si\ O_{21}\ ^{W}F$ as the root composition. The principal substitutions (involving cations) relating other end-members to the root composition are given in Table 4.

The *T*(3) site contains three constituents (Si, B, Be), and there are three additional independent compositional variables: ^{X}Mg, ^{M}Al and ^{T}Si; so how do we represent these end-members, together with the variation in composition of kornerupine *sensu lato*, in a user-friendly graphical form? If we omit Be-bearing kornerupine (which is rare, Cooper *et al.* 2009c), we can reduce the eight end-members in Table 3 to six. Furthermore, if we condense the *T*- and *V*-group species (and designate them as *T*-group species), we reduce the system to three independent variables, ^{X}Mg, ^{M}Al and ^{T}Si, and four end-members (Table 5).

As discussed by Cooper *et al.* (2009b), a locally occupied *X*-site requires a vacancy at the locally associated H sites, and hence F must occur at the locally associated O(10) site. Thus compositions with *X* = 1.0 Mg must have *W* = 1.0 F. This restriction is accommodated in the end-member compositions given above.

As noted above, we have identified three compositional variables: ^{X}Mg, ^{M}Al and ^{T}Si that span the four end-members (1), (2), (5) and (6) given above; this space is illustrated in Figure 15. The end-member compositions (1), (2), (5) and (6) are coplanar in Figure 15, and hence we can represent all end-members (and all compositional variation) of kornerupine in two dimensions, using end-member (1) as the origin and the exchange reactions [1] and [2] as orthogonal axes. The exchanges [1] and [2] are independent; however,

TABLE 3. PRINCIPAL HETEROVALENT END-MEMBERS FOR KORNERUPINE

	X	*Y*	*M*	*T*	*V*		*W*
(1)	□	Mg_2	(Al_5Mg_2)	Si_4	Si	O_{21}	F
(2)	□	Mg_2	Al_7	(Si_3B)	B	O_{21}	F
(3)	□	Mg_2	Al_7	(Si_2B_2)	Si	O_{21}	F
(4)	□	Mg_2	Al_7	Si_4	Be	O_{21}	F
(5)	Mg	Mg_2	(Al_5Mg_2)	Si_4	Si	O_{21}	F
(6)	Mg	Mg_2	Al_7	(SiB_3)	B	O_{21}	F
(7)	Mg	Mg_2	Al_7	B_4	Si	O_{21}	F
(8)	Mg	Mg_2	Al_7	(Si_2B_2)	Be	O_{21}	F

Mg = $^{[8,6]}$(Mg,Fe^{2+}): Al = $^{[6]}$(Al,Fe^{3+}); Si = $^{[4]}$Si; B = $^{[4]}$(Al,B); Be = $^{[4]}$Be; F = (OH) + F for compositions (1)–(4) and F = F for compositions (5)–(8).

TABLE 4. PRINCIPAL SUBSTITUTIONS (INVOLVING CATIONS) RELATING OTHER END-MEMBERS TO THE ROOT COMPOSITION OF KORNERUPINE SENSU STRICTO

X	*M*	*T*	*V*		*X*	*M*	*T*	*V*	Exchange
–	Mg_2	Si	Si	→	–	Al_2	B	B	$^{M}Al_2 + {}^{T}B + {}^{V}B \rightarrow {}^{M}Mg_2 + {}^{T}Si + {}^{V}Si$
–	Mg	Si	–	→	–	Al	B	–	$^{M}Al + {}^{T}B \rightarrow {}^{M}Mg + {}^{T}Si$
–	Mg_2	–	Si	→	–	Al_2	–	Be	$^{M}Al_2 + {}^{V}Be \rightarrow {}^{M}Mg_2 + {}^{V}Si$
□	Al_2	–	–	→	Mg	Mg_2	–	–	$^{X}Mg + {}^{M}Mg_2 \rightarrow {}^{X}\square + {}^{M}Al_2$
□	Mg_2	Si_3	Si	→	Mg	Al_2	B_3	B	$^{X}Mg + {}^{M}Al_2 + {}^{T}B_3 + {}^{V}B \rightarrow {}^{X}\square + {}^{M}Mg_2 + {}^{T}Si_3 + {}^{V}Si$
□	Mg_2	Si_4	–	→	Mg	Al_2	B_4	–	$^{X}Mg + {}^{M}Al_2 + {}^{T}B_4 \rightarrow {}^{X}\square + {}^{M}Mg_2 + {}^{T}Si_2$
□	Mg_2	Si_2	Si	→	Mg	Al_2	B_2	Be	$^{X}Mg + {}^{M}Al_2 + {}^{T}B_2 + {}^{V}Be \rightarrow {}^{X}\square + {}^{M}Mg_2 + {}^{T}Si_2 + {}^{V}Si$

exchange [3] is a linear combination of [1] × 2 and [2]. Next, we must derive the relations between the chemical composition of kornerupine and the coordinate system in the plane (1)(2)(5)(6) of Figure 15.

Let us write the amounts x, y, z of end-member compositions (1), (2) and (5) as follows:

(1) $^{X}\square\ ^{Y}Mg_2\ ^{M}Al_5Mg_2\ ^{T}Si_5\quad O_{21}\ F\ x$

(2) $^{X}\square\ ^{Y}Mg_2\ ^{M}Al_7\quad\ ^{T}Si_3B_2\ O_{21}\ F\ y$

(5) $^{X}Mg\ ^{Y}Mg_2\ ^{M}Al_3Mg_4\ ^{T}Si_5\quad O_{21}\ F\ z$

We may express the principal compositional variables ^{X}Mg, ^{M}Al and ^{T}Si for any kornerupine composition as follows:

$$z = {}^{X}\mathrm{Mg} \quad (4)$$

$$5x + 7y + 3z = {}^{M}\mathrm{Al} \quad (5)$$

$$5x + 3y + 5z = {}^{T}\mathrm{Si} \quad (6)$$

We may solve equations (4–6) for x, y and z as follows:

$$x = (7\ {}^{T}\mathrm{Si} - 3\ {}^{M}\mathrm{Al} - 26\ {}^{X}\mathrm{Mg}) / 20$$

$$y = ({}^{M}\mathrm{Al} + 2\ {}^{X}\mathrm{Mg} - {}^{T}\mathrm{Si}) / 4$$

$$z = {}^{X}\mathrm{Mg}$$

and express the composition of kornerupine in terms of end-members (1), (2) and (5) in the ternary system of Figure 16, where the compositions of kornerupine crystals K1 → K52 (Cooper *et al.* 2009a) are shown.

Principal Homovalent Chemical Variations: Bulk Composition

The principal homovalent chemical variations in kornerupine *sensu lato* are ^{T}Al ⇌ ^{T}B, and ^{X,M} Fe^{2+} ⇌ ^{X,M} Mg (Figs. 3a,b). Other homovalent variations involve Fe^{3+} ⇌ Al, Mn^{2+} ⇌ Mg, and F ⇌ OH, plus others involving minor amounts of transition metals. The extent of variations ^{T}Al ⇌ ^{T}B, and ^{X,M} Fe^{2+} ⇌ ^{X,M} Mg is shown in Figures 17a and 18 for the data of Cooper *et al.* (2009a). What is immediately apparent on inspection of Figures 17a and 18 is that there are linear relations between ^{T}Al and ^{T}B and between ^{X,M} Fe^{2+} and ^{X,M} Mg, but the slopes of the regression lines through

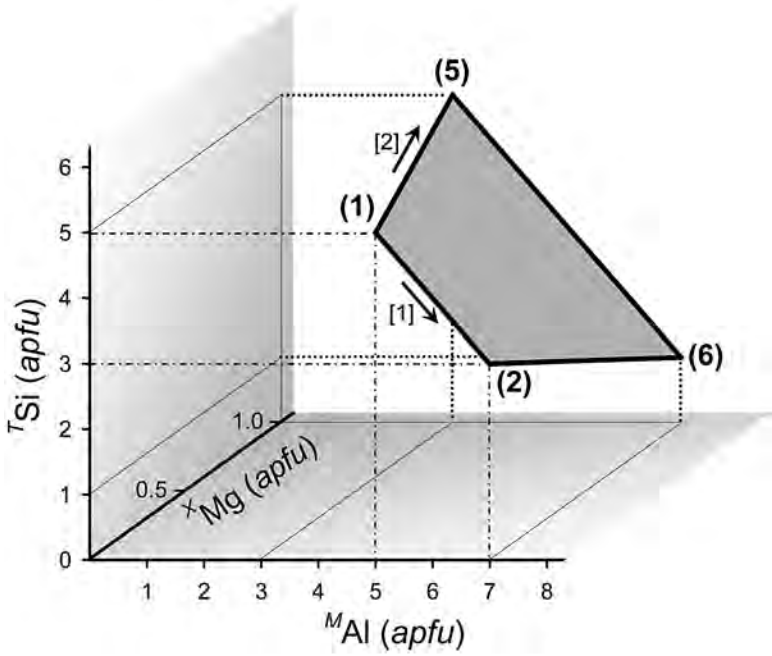

FIG. 15. The end-member compositions (1) □ Mg_2 Al_5 Mg_2 Si_5 O_{21} F, (2) □ Mg_2 Al_7 Si_3 B_2 O_{21} F, (5) Mg Mg_2 Al_3 Mg_4 Si_5 O_{21} F, (6) Mg Mg_2 Al_7 Si B_4 O_{21} F in the coordinate system ^{T}Si, ^{M}Al, ^{X}Mg; the grey-shaded area shows the plane spanning these four compositions.

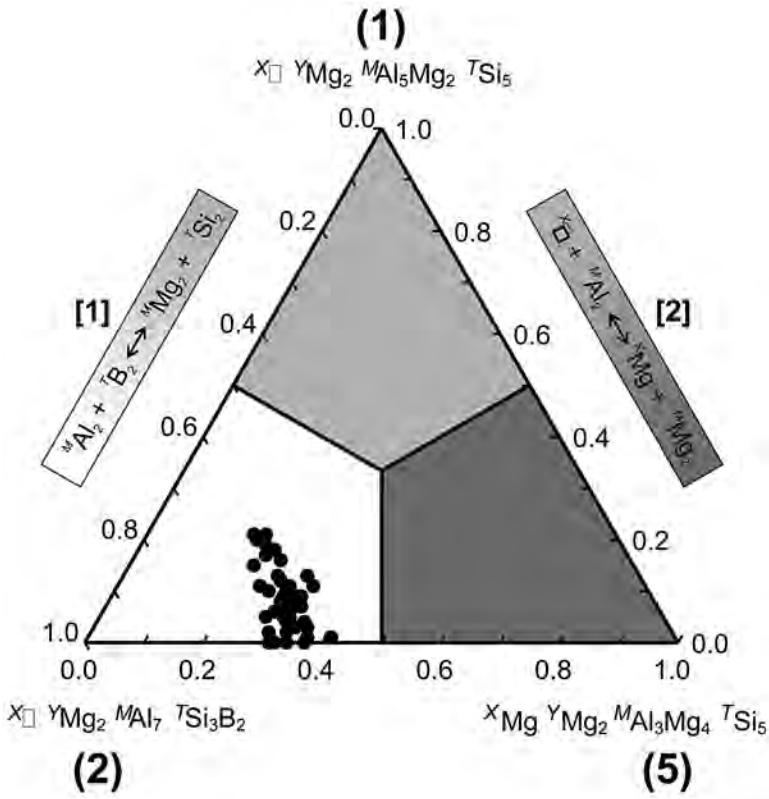

FIG. 16. The chemical compositions of the kornerupine samples of Cooper *et al.* (2009a) shown in the ternary system $^{X}\square\ ^{Y}Mg_2\ ^{M}Al_5Mg_2\ ^{T}Si_5$ – $^{X}\square\ ^{Y}Mg_2\ ^{M}Al_7\ ^{T}Si_3B_2$ – $^{X}Mg\ ^{Y}Mg_2\ ^{M}Al_3Mg_4\ ^{T}Si_5$.

TABLE 5. PRINCIPAL SUBSTITUTIONS (INVOLVING CATIONS) IN Be-FREE KORNERUPINE RELATING OTHER END-MEMBERS TO THE ROOT COMPOSITION

	X	*Y*	*M*	*T**		*W*	Exchange	
(1)	□	Mg_2	Al_5Mg_2	Si_5	O_{21}	F		
(2) ≡ (3)	□	Mg_2	Al_7	Si_3B_2	O_{21}	F	$^{M}Al_2 + {}^{T}B_2 \rightarrow {}^{M}Mg_2 + {}^{T}Si_2$	[1]
(5)	Mg	Mg_2	Al_3Mg_4	Si_5	O_{21}	F	$^{X}Mg + {}^{M}Mg_2 \rightarrow {}^{X}\square + {}^{M}Al_2$	[2]
(6) ≡ (7)	Mg	Mg_2	Al_7	SiB_4	O_{21}	F	$^{X}Mg + {}^{M}Al_2 + {}^{T}B_4 \rightarrow {}^{X}\square + {}^{M}Mg_2 + {}^{T}Si_4$	[3]

* Note that the *T*- and *V*-group species have been condensed into one (*T*) group.

the data are *not* unity [as was suggested by Klaska & Grew (1991) for ^{T}Al and ^{T}B].

Both of these chemical variations are particularly complicated in kornerupine owing to additional atoms at these sites of different formal charge. Thus Al and B show correlated variation at the *T* sites, and the other cation at the *T* sites is Si, with a different formal charge. As the slope of the ^{T}Al *versus* B correlation is not unity, the total amount of trivalent cations (*i.e.*, ^{T}Al + B) varies with variation in the ^{T}Al : B ratio, and hence the Si site population changes also, under the constraint that ^{T}Al + B + Si = 5 *apfu*. Thus there is a change in the total charge at the *T* sites as the ^{T}Al : B ratio varies. So we have the curious situation that a homovalent chemical variation results in a change in the aggregate charge at the constituent sites. A similar situation occurs at the *X*

+ *M* sites, where variation in the $^{X+M}Fe^{2+}$: ^{X+M}Mg ratio correlates with change in $^{X+M}$(Fe + Mg), and hence with a change in the ^{M}Al or $^{X}\square$content. Of course, neither of these chemical exchanges is strictly homovalent, as each involves a correlated heterovalent substitution at the same group of sites.

Al → B at the T sites

As the stoichiometry of kornerupine constrains ^{T}Al + B + Si to be equal to 5 *apfu*, the linear relation between ^{T}Al and B (Fig. 17a) requires that there is also a linear correlation with respect to Si [corresponding ^{T}Si values (*apfu*) are indicated over the data range]. The relation between ^{T}Al and B is displaced above, and at a greater slope than the simple 1 : 1 reference line passing through B = 1.0 *apfu*.

As shown by Cooper *et al.* (2009a), although B occurs only at the *T*(3) site, Al occurs at the *T*(1), *T*(2) and *T*(3) sites, each of which shows variable Al content (Fig. 6). The kornerupine structure has two distinct arrangements of tetrahedra, the *T*(1)–*T*(1) dimer and the *T*(2)–*T*(3)–*T*(2) trimer, and these motifs do not link directly to each other (Fig. 2). We can factor the variation of B and $^{(T+V)}$Al (Fig. 17a) into the analogous variations within these dimeric and trimeric units, as shown in Figures 17b and 17c, respectively. The variation in Al as a function of B is linear in each silicate unit, with the following relations:

$$^{T(1)}\text{Al} = 0.19(1)–0.207(8)\ \text{B} \qquad R^2 = 0.93$$

$$^{T(2)\,+\,T(3)}\text{Al} = 1.20(5)–1.02(3)\ \text{B} \qquad R^2 = 0.97$$

It is notable that for the *T*(2)–*T*(3)–*T*(2) trimer (Fig. 17c), the slope of the relation is 1.0, and that there is a near-zero net variation in Si content over the *T*(2)–*T*(3)–*T*(2) trimer [note that the $^{T(2)}$Si and $^{T(3)}$Si variations with increasing B are nearly mirror images of each other (Fig. 6) and show a simple 1 : 1 inverse relation $^{T(2)}$Si = 1.83(5) – 1.03(4)$^{T(3)}$Si, R^2 = 0.94]. This is consistent with dominant B → Si substitution at *T*(3) coupled to Si → Al substitution at *T*(2) on a *pfu* basis, so as to avoid B–O–Al bridges (Klaska & Grew 1991). In the *T*(1)–*T*(1) dimer, there is no B present, and hence

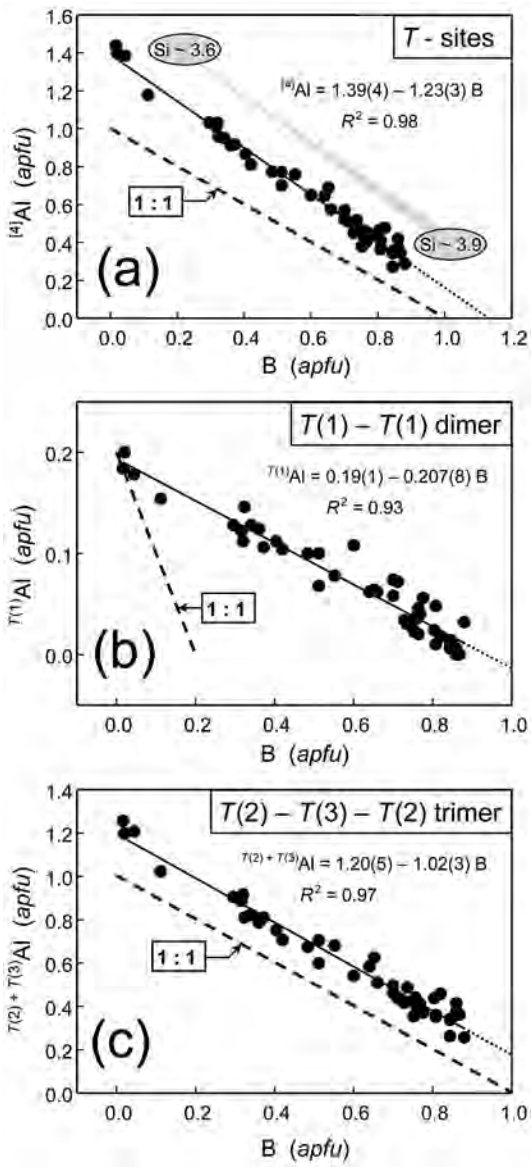

FIG. 17. (a) Variation in (a) $^{[4]}$Al, (b) $^{T(1)}$Al and (c) $^{T(2)+T(3)}$Al as a function of B.

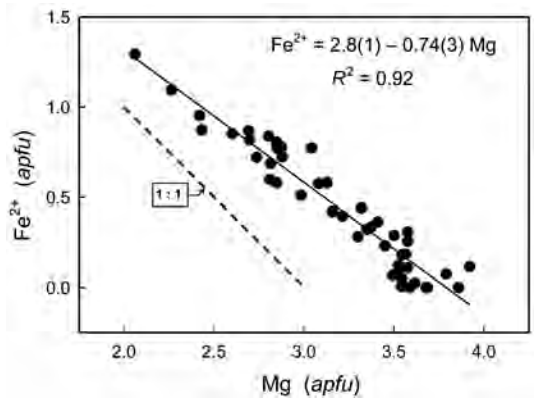

FIG. 18. Variation in Fe^{2+} as a function of Mg in the kornerupine crystals of this study.

the correlation of Al with B (Fig. 17b) must be due to some inductive effect [in accord with the much lower slope (<<1.0) for this correlation]. Thus we see that the deviation of the slope from 1.0 in Figure 17a is due to the induced correlation of Al in the *T*(1)–*T*(1) dimer (Fig. 17b) with variation in B content of the *T*(2)–*T*(3)–*T*(2) trimer. Extrapolation of the ^{T}Al–B variation in Figure 17a to a $B_{1.0}$ composition does not support an entirely $^{[4]}$Al-free $^{T}Si_{4.0}B_{1.0}$ end-member composition [excess ^{T}Al would reside at the *T*(2)–*T*(3)–*T*(2) trimer (Fig. 17c)].

Fe^{2+} → Mg at the X and M sites

The situation for this substitution is somewhat different from that at the *T* sites, as two distinct types of sites are involved (the $^{[8]}$*X* and $^{[6]}$*M* sites), and the other principal substituents of these two site groups differ, being □ at the *X* site and Al at the *M* sites. Thus the stoichiometric constraint may be written as Fe^{2+} + Mg + □ + Al(Fe^{3+}) = 10 *apfu*, and the linear relation between Fe^{2+} and Mg (Fig. 18) does not intrinsically constrain □ and Al to any correlated values. There is a poor inverse correlation between □ and Mg, but nothing that resembles the correlations of Figures 17a and 18.

Let us consider the principal sites at which this substitution occurs: *M*(1), *M*(2) and *X* (Table 2); both *M*(3) and *M*(5) are almost completely occupied by Al, with only minor (< 0.1 *apfu*) Mg content. As shown in Figures 1 and 2, all of the *M* sites involved in significant substitution of Mg and Fe^{2+} occur in the B layer of the structure; only the *X* site occurs in the A layer (Fig. 1a). Thus substitution of Fe^{2+} for Mg will increase the size of the B layer relative to that of the A layer, as Fe^{2+} (r = 0.78 Å, Shannon 1976) is significantly larger than Mg (r = 0.72 Å). As the crystal structure of kornerupine consists of A and B layers stacked in the *b* direction, any expansion of components of one layer must be accompanied by (1) shrinkage of other components of the same layer, or (2) expansion of the other layer, in order to conserve commensurability. As the A layer shows far less chemical variability than the B layer, potential increase in size of the *M*(1) and *M*(2) octahedra with increasing $^{M}Fe^{2+}$ must be compensated by increasing ^{M}Al at *M*(2) and *M*(4) in order to maintain the dimensional correspondence of the B layer with the A layer. Hence the substitution Fe^{2+} → Mg is accompanied by the substitution Al → Mg, accounting for the unusually low slope (–0.74) of the relation between Fe^{2+} and Mg (Fig. 18). Note that for simplicity, we have not considered the effect of the *X* site on this relation. However, if this is done, analogous results are obtained.

F → (OH) at the W site

Cooper *et al.* (2009b) showed that where the *W* site is locally occupied by (OH), the associated H atom occurs too close to one of the two adjacent *X* sites for that site to be occupied. Hence in a crystal where *W* = (OH), the *X* site cannot be more than half-occupied. Where the *W* site is locally occupied by F, the two adjacent X sites have no constraint on their occupancy resulting from the *W* site. Hence in a crystal where *W* = F, the *X* site can (in principle) be completely occupied. Of course, there are other constraints on the occupancy of the *X* site, but the local stereochemistry of the *X* and *W* sites constrain the occupancy of the *X* site to be ≤ (1 + F) / 2 *apfu*.

Grew *et al.* (1996) showed that F is very restricted in kornerupine *sensu stricto* (generally less than 0.06 *apfu*), whereas it can reach up to 0.38 *apfu* in prismatine. As prismatine commonly shows higher Fe contents, there is a very weak positive correlation between Fe^{2+} and F (not shown), the origin of which is not clear at the moment. There seems to be little crystal-chemical constraint on the extent of (OH) ⇌ F variation in kornerupine *sensu lato*.

Site-Specific Heterovalent Chemical Variations

As noted above, three independent compositional variables, ^{X}Mg, ^{M}Al and ^{T}Si, are required to express the heterovalent chemical variation within the (Be-free) kornerupine structure. We will now examine their variation on a site-specific basis. The compositional variables $^{T(1)}$Si, $^{T(2)}$Si, $^{M(2)}$Al and ($^{M(3)}$Al + $^{M(5)}$Al) are shown as functions of $^{T(3)}$Si in Figure 19. The data for $^{T(1)}$Si, $^{T(2)}$Si and $^{M(3)+M(5)}$Al show (somewhat scattered) inverse linear correlations with $^{T(3)}$Si, whereas $^{M(2)}$Al shows a positive correlation with $^{T(3)}$Si. The fields of data in Figure 19 are also shaded to show the range in Fe*, which is highly correlated with $^{T(3)}$Si, $^{T(1)}$Si and $^{T(2)}$Si (as also indicated in Fig. 9). On an individual-site basis, $^{M(3)}$Al and $^{M(5)}$Al show correlations similar to that of ($^{M(3)}$Al + $^{M(5)}$Al) (Fig. 19d).

The remaining sites involved in heterovalent substitutions are *M*(4) and *X*; $^{M(4)}$Al and ^{X}Mg are shown as functions of $^{T(3)}$Si in Figures 20a and 20b; note that ^{X}Mg is plotted in terms of charge *pfu* relative to vacancy. Figures 20a and 20b have similar distributions of data, and the relative positioning of the labels A, B, C (denoting specific crystals; A: K11, B: K41, C: K40), indicate a sympathetic relation between $^{M(4)}$Al ⇌ $^{M(4)}$Mg and ^{X}Mg ⇌ ^{X}□, whose extent is a function of $^{T(3)}$Si content [*i.e.*, at low $^{T(3)}$Si (or high B) content, these substitutions are more extensive than at high $^{T(3)}$Si content]. The sum ($^{M(4)}$Al + ^{X}Mg) is shown as a function of $^{T(3)}$Si in Figure 20c; the broad field of data indicates a weak positive correlation. The changes in charge distribution (*pfu*) at the various sites that occur with the observed maximum range in $^{T(3)}$Si → $^{T(3)}$(B) are given in Table 6 and Figures 19 and 20c. The net increase in charge of 0.35^{+} over *M*(4) *and X* offsets the 0.35^{-} charge

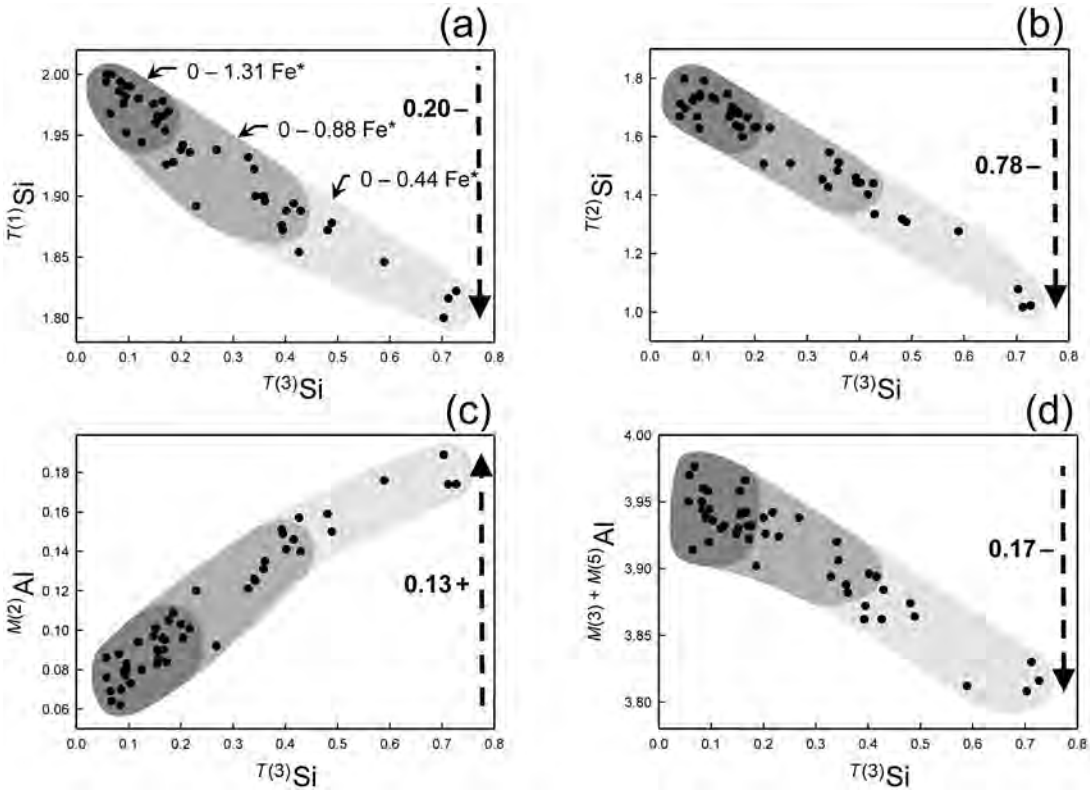

FIG. 19. Variation in (a) $^{T(1)}$Si, (b) $^{T(2)}$Si, (c) $^{M(2)}$Al and (d) $^{M(3)+M(5)}$Al as a function of $^{T(3)}$Si in kornerupine. The broken arrows show the net change in the ordinate with increasing $^{T(3)}$Si.

deficit at the other sites. The relations between ^{X}Mg, $^{M(4)}$Al and $^{T(3)}$Si are shown in Figure 21. At high values of $^{T(3)}$Si (low B), the substitutions ^{X}Mg ⇌ $^{X}\square$ and $^{M(4)}$Al ⇌ $^{M(4)}$Mg are limited in extent, whereas at low values of $^{T(3)}$Si (high B), the extent of these heterovalent substitutions is large. There is a negative correlation between ^{X}Mg and $^{M(4)}$Al at low $^{T(3)}$Si (high B) [*i.e.*, data lying near and parallel to the black arrow labeled (1)]. Figure 21 is important in showing how the *X*, *M*(4) and *T*(3) sites combine in their heterovalent substitutions. All net changes in $^{T(3)}$Si are coupled to simple heterovalent substitutions at $^{T(1)}$Si, $^{T(2)}$Si, $^{M(2)}$Al, $^{M(3)}$Al and $^{M(5)}$Al (Fig. 19). The resulting site-specific chemical exchanges (*pfu* basis) are given in Table 7. The three principal heterovalent substitutions ^{X}Mg → $^{X}\square$, $^{M(4)}$Al → $^{M(4)}$Mg and $^{T(3)}$Si → $^{T(3)}$B are expressed as three separate pairings [exchanges (1)–(3)], and labeled similarly on Figure 21. Exchange (1) is neutral, and can only be extensive in kornerupine at low $^{T(3)}$Si values (high B); the most extensive substitution at *X or M*(4) and *T*(3) [exchanges (2) or (3)] occurs at either high $^{M(4)}$Al *or* high ^{X}Mg values, respectively. Exchanges (2) or (3) involve substitution at the *T*(3) site, and must couple to heterovalent substitutions (i–iv) at other sites, so that overall electroneutrality is maintained (Table 7).

TABLE 6. SITE-SPECIFIC HETEROVALENT SUBSTITUTIONS

Site	Substitution			Charge (*pfu*)	Net charge
T(3)	Si	→	B*	0.67+	
T(2)	Al	→	Si	0.78–	
T(1)	Al	→	Si	0.20–	0.35–
M(2)	Al	→	Mg	0.13+	
M(3,5)	Mg	→	Al	0.17–	
M(4)	Al	→	Mg	0.44 Δ**	0.35+
X	Mg	→	□	0.44 Δ	

* B: includes $^{[4]}$(B,Al); ** see Figure 21a; the net change in charge is less than expected from these charges as the substitutions shown in Figure 21 are partly correlated.

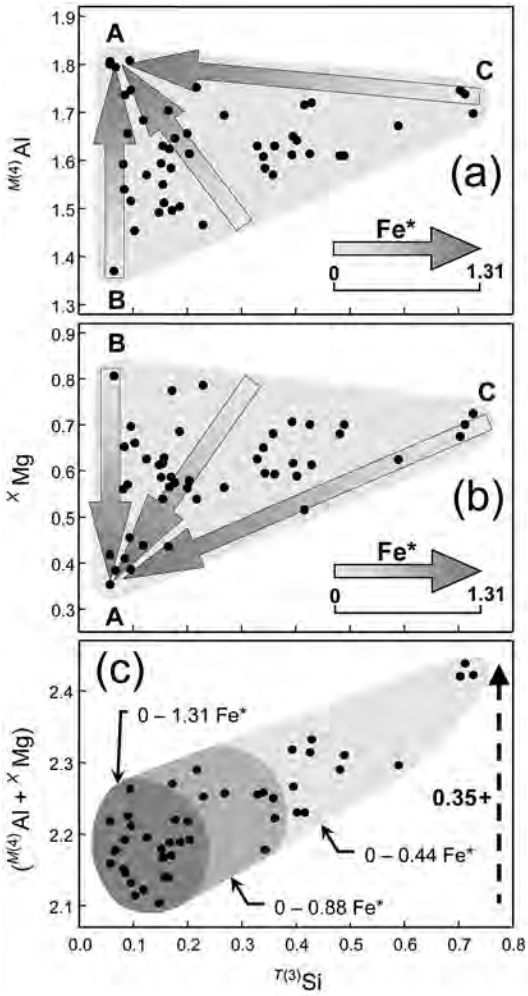

FIG. 20. Variation in (a) $^{M(4)}$Al, (b) ^{X}Mg and (c) $^{M(4)}$Al + ^{X}Mg as a function of $^{T(3)}$Si in kornerupine. The broken arrow shows the net change in the ordinate with increasing $^{T(3)}$Si.

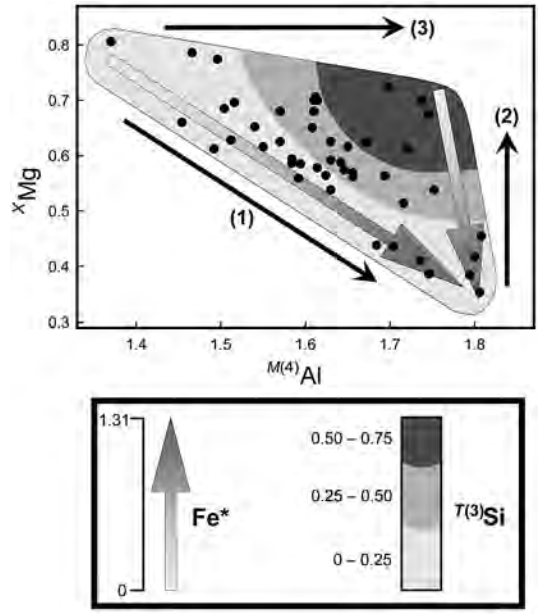

FIG. 21. Variation in ^{X}Mg as a function of $^{M(4)}$Al in kornerupine.

TABLE 7. HETEROVALENT SITE-SPECIFIC CHEMICAL EXCHANGES

	Substitution								Change in net charge
(1)*	$^{X}\square$	+	$^{M(4)}Al_2$	=	^{X}Mg	+	$^{M(4)}Mg_2$		[0]*
(2)	^{X}Mg	+	$^{T(3)}Si$	=	$^{X}\square$	+	$^{T(3)}B$		[3⁻]
(3)	$^{M(4)}Al_2$	+	$^{T(3)}Si$	=	$^{M(4)}Mg_2$	+	$^{T(3)}B$		[3⁻]
(i)	$^{T(1)}Al_2$	+	$^{T(3)}Si$	=	$^{T(1)}Si_2$	+	$^{T(3)}B$		[1⁺]
(ii)	$^{T(2)}Al_2$	+	$^{T(3)}Si$	=	$^{T(2)}Si_2$	+	$^{T(3)}B$		[1⁺]
(iii)	$^{M(2)}Al$	+	$^{T(3)}Si$	=	$^{M(2)}Mg$	+	$^{T(3)}B$		[2⁻]
(iv)	$^{M(3,5)}Mg_4$	+	$^{T(3)}Si$	=	$^{M(3,5)}Al_4$	+	$^{T(3)}B$		[3⁺]
								$\Sigma_{(i-iv)}$	3⁺

* The numbers refer to the arrows shown in Figure 21.

Dependent homovalent Fe ⇌ Mg

The differently shaded fields on Figures 19 and 20c show approximate ranges of Fe* (Fe* = Fe^{2+} + Mn^{2+}). At high $^{T(3)}$Si values (*i.e.*, > 0.4 $^{T(3)}$Si *pfu*), all kornerupine crystals have low Fe* (0 – 0.44 Fe* *apfu*). At low $^{T(3)}$Si values (*i.e.*, < 0.2 $^{T(3)}$Si *pfu*), the maximum range in Fe* (0 – 1.31 Fe* *apfu*) is observed. The shaded arrows on Figures 20a, b and 21 show approximate *progressive* changes in Fe* as a function of $^{T(3)}$Si, $^{M(4)}$Al and ^{X}Mg. It is apparent that greater $^{M(4)}$Al → $^{M(4)}$Mg *and* $^{X}\square$ → ^{X}Mg , in combination with $^{T(3)}$B → $^{T(3)}$Si , combine with greater Fe → Mg at the *X*, *M*(1) and *M*(2) sites collectively. The extent of homovalent Fe^{2+} → Mg thus correlates with these site-specific heterovalent exchanges.

Let us examine the sites at which Fe^{2+} → Mg replacement occurs: *M*(1), *M*(2) and *X*. As shown in Figures 1b and 2, *M*(1) and *M*(2) occur in the B layer of the structure, and Fe^{2+} → Mg replacement will increase the size of these octahedra. As the total Fe^{2+} content increases, we saw earlier that the degree of Fe^{2+}–Mg order is similar at the *M*(1) and *M*(2) sites (Fig. 12b). Simultaneous expansion of the *M*(1) and *M*(2) octahedra as a result of Fe^{2+} → Mg replacement is accompanied

by mutual contraction of: (1) the *T*(3) tetrahedron that bridges *M*(1)–*M*(1) corner-sharing dimers, and (2) the *M*(4) octahedron that shares edges with both the *M*(1) and *M*(2) octahedra (Fig. 2). Contraction of the *T*(3) and *M*(4) polyhedra occurs through the heterovalent exchanges $^{T(3)}B \rightarrow {}^{T(3)}Si$ and $^{M(4)}Al \rightarrow {}^{M(4)}Mg$, respectively. The role of the *X* site in facilitating Fe → Mg exchange *via* $^{X}\square \rightarrow {}^{X}Mg$ replacement is less obvious. A single $^{[8]}X$ site shares four of its polyhedron edges [O(4)–O(10)] with four neighboring *M*(1) octahedra, and another four edges [O(4)–O(9)] with four adjacent *T*(1) tetrahedra. Where the *X* site is vacant, its polyhedron edges can adjust more easily to the neighboring environment. This freedom can be seen along the O(4)–O(10) edge of the *M*(1) octahedron, and indirectly at the *M*(2) octahedron along its O(3)–O(3) edge *via* adjustment of the *T*(1)–O(9)–*T*(1) angle (Fig. 2).

Site-specific substitution: summary

Both heterovalent and homovalent site-specific substitutions can be summarized in the following way:

(1) $^{T(3)}Si \rightarrow {}^{T(3)}B$ couples to $^{T(1,2)}Al \rightarrow {}^{T(1,2)}Si$, which increases the sizes of the tetrahedra within the B layer. Linkage of the A layer to the B layer is facilitated through expansion of the A layer *via* the substitution $^{M(3,5)}Mg \rightarrow {}^{M(3,5)}Al$. Only minor expansion of the structure occurs along the *c* axis owing to coupled contraction of the *M*(2) octahedron [$^{M(2)}Al \rightarrow {}^{M(2)}Mg$] and sterically induced distortion of the *M*(1) and *M*(4) octahedra (Figs. 1, 2).

(2) At high values of $^{T(3)}Si$ (*i.e.*, low B), the B layer (of tetrahedra) of the structure shows maximum distension, which imparts the greatest restriction upon the composition of the A layer [the *M*(1)–*M*(2)–*M*(3)–*M*(4)–*M*(5) wall of edge-sharing octahedra] (Fig. 2). As such, the ranges of the $^{X}Mg \rightleftharpoons {}^{X}\square$ and $^{M(4)}Al \rightleftharpoons {}^{M(4)}Mg$ substitutions are limited in their extent (Fig. 21).

(3) At low values of $^{T(3)}Si$ (*i.e.*, high B), the B layer of the structure is smaller, allowing more compositional freedom to the A layer (*i.e.*, a smaller B layer promotes linkage between layers). In addition to more extensive $^{X}Mg \rightleftharpoons {}^{X}\square$ and $^{M(4)}Al \rightleftharpoons {}^{M(4)}Mg$ substitution, a smaller tetrahedral component also allows greater variation in homovalent $^{M(1,2)}Fe^{2+} \rightleftharpoons {}^{M(1,2)}Mg$ variation (Fig. 21).

Summary

(1) The chemical formula of kornerupine *sensu lato* may be written as

$$X\ Y_2\ M_7\ T_4\ V\ O_{21}\ W$$

where the corresponding sites are shown to the right below:

$X = \square$, Mg, Fe^{2+}	*X*
Y = Mg, Fe^{2+}	*M*(1)
M = Al, Mg, Fe^{2+}, Fe^{3+}	*M*(2), *M*(3), *M*(4), *M*(5)
T = Si, Al	*T*(1), *T*(2)
V = Si, Al, B, Be	*T*(3)
W = OH, F	O(10)

(2) The total number of cations is variable (14.2 to 14.4 *apfu*), the sum of the cation charge is 43+, and the amount of vacancy (*pfu*) is given by

$$\square = 43 - 4S^{4+} - 3S^{3+} - 2S^{2+}$$

(3) The degree of (Si, Al) order at the *T* sites is strongly correlated to the B content according to the following coupled substitution:

$$^{T(1)}Si_{0.2} + {}^{T(2)}Si_{0.8} + {}^{T(3)}B(Al)_{0.7} \rightleftharpoons {}^{T(1)}Al_{0.2} + {}^{T(2)}Al_{0.8} + {}^{T(3)}Si_{0.7}$$

which operates with a net charge gain (or deficit) of 0.3+ *pfu* for the kornerupine samples studied.

(4) The *T*-site populations are coupled to both B and Fe^{2+} content; at moderate Si content (~3.71 Si *apfu*), the structure accommodates the largest range in B (0–0.9 *apfu*) and Fe^{2+} (0–1.3 *apfu*).

(5) Flexibility in the kornerupine structure originates at the *T*(2)–*T*(3)–*T*(2) trimer, where coupled expansion–contraction of tetrahedra and rotation [*T*(2)] proceed at the expense of sterically induced distortion of the neighboring *M*(1) and *M*(4) octahedra.

(6) Both Fe^{2+} and Mg are approximately disordered over *M*(1) and *M*(2), with the maximum [$^{M(1)}Fe^{2+}$ + $^{M(2)}Fe^{2+}$] content coupled to the B content of the crystal. The *X* site shows the greatest affinity for Fe^{2+}, with no apparent coupling of $^{X}Fe^{2+}$ to the B content. The maximum allowed $Fe^{2+}(Mn^{2+})$ in kornerupine is estimated at 1.60 *apfu*.

(7) The range of homovalent substitution $Fe^{2+} \rightleftharpoons Mg$ is most extensive where coupled to $^{X}\square + {}^{M}Al_2 \rightarrow {}^{X}Mg + {}^{M}Mg_2$, and is maximal at high $^{T(3)}B$ (> ⅔ B *apfu*) and moderate ^{T}Si (~3.71 Si *apfu*) contents.

(8) The Al contents of *M*(2) and *M*(3) + *M*(5) are strongly negatively and positively correlated, respectively, with B content.

(9) The trivalent-cation content M^{3+} (= Al + Fe^{3+} + Cr + V + Ti^{4+}) of the *M*(4) site is linearly related to the □ and Si contents of the crystal.

(10) Combining the *T* and *V* sites, the principal (heterovalent) end-member compositions for Be-free crystals are as follows:

X	*Y*	*M*	*T*		*W*
□	Mg_2	Al_5Mg_2	Si_5	O_{21}	F
□	Mg_2	Al_7	Si_3B_2	O_{21}	F
Mg	Mg_2	Al_3Mg_4	Si_5	O_{21}	F
Mg	Mg_2	Al_7	SiB_4	O_{21}	F

(11) These compositions can be represented in the orthogonal system ^{X}Mg–^{M}Al–^{T}Si, and define a plane on which the compositions of all samples of kornerupine examined here (which covers the range of all known compositions) can be graphically represented. Chemical variation involving two of the three independent compositional variables is as follows:

$$^{X}\square + {}^{M}Al_2 = {}^{X}Mg + {}^{M}Mg_2$$

$$^{M}Mg + {}^{T}Si = {}^{M}Al + {}^{T}B$$

where maximum variation at the *X* and *M* sites [$^{X}\square$ + $^{M}Al_2$ = ^{X}Mg + $^{M}Mg_2$] occurs at high $^{T(3)}$B (> ⅔ B *apfu*) and moderate ^{T}Si (~3.71 Si *apfu*) contents.

(12) The principal homovalent chemical variations in kornerupine are ^{T}Al ⇌ ^{T}B and $^{X,M}Fe^{2+}$ ⇌ ^{X,M}Mg. However, neither show a simple 1:1 substitution. For ^{T}Al ⇌ ^{T}B, the total amount of trivalent cations (*i.e.*, ^{T}Al + B) varies with the ^{T}Al:B ratio (and hence with a change in the Si content). For $^{X,M}Fe^{2+}$ ⇌ ^{X,M}Mg, the total amount of divalent cations (*i.e.*, $^{X+M}Fe^{2+}$ + $^{X+M}$Mg) varies with $^{X+M}Fe^{2+}$: $^{X+M}$Mg ratio (and hence with a change in the ^{M}Al or $^{X}\square$ content). However, the slopes of ensuing relations are significantly less than unity, as these substitutions are constrained by commensurability requirements arising from the layered nature of the structure and the distribution of sites over which these substitutions act.

(13) On a site basis, the most important heterovalent chemical variations are as follows:

(1) $^{X}\square + {}^{M(4)}Al_2 = {}^{X}Mg + {}^{M(4)}Mg_2$

(2) $^{X}Mg + {}^{T(3)}Si = {}^{X}\square + {}^{T(3)}B$

(3) $^{M(4)}Al_2 + {}^{T(3)}Si = {}^{M(4)}Mg_2 + {}^{T(3)}B$

Substitution (1) is neutral, and (2) and (3) are linearly coupled to each of the following substitutions:

(i) $^{T(1)}Al_2 + {}^{T(3)}Si = {}^{T(1)}Si_2 + {}^{T(3)}B$

(ii) $^{T(2)}Al_2 + {}^{T(3)}Si = {}^{T(2)}Si_2 + {}^{T(3)}B$

(iii) $^{M(2)}Al + {}^{T(3)}Si = {}^{M(2)}Mg + {}^{T(3)}B$

(iv) $^{M(3,5)}Mg_4 + {}^{T(3)}Si = {}^{M(3,5)}Al_4 + {}^{T(3)}B$

Acknowledgements

We thank Gianni Andreozzi, Sergio Lucchesi and Ron Peterson for their perspicacious comments on this paper. This work was supported by a Canada Research Chair, Research Tools and Equipment, Discovery and Major Facilities Access grants to FCH from the Natural Sciences and Engineering Research Council of Canada, and Innovation Grants from the Canadian Foundation for Innovation to FCH.

References

Cooper, M.A. & Hawthorne, F.C. (2009): The crystal chemistry of the kornerupine–prismatine series. IV. Complete chemical formulae from electron-microprobe data and X-ray powder diffraction. *Can. Mineral.* **47**, 297-302.

Cooper, M.A., Hawthorne, F.C. & Grew, E.S. (2009a): The crystal chemistry of the kornerupine–prismatine series. I. Crystal structure and site populations. *Can. Mineral.* **47**, 233-262.

Cooper, M.A., Hawthorne, F.C. & Grew, E.S. (2009c): The crystal chemistry of the kornerupine–prismatine series. V. The siting of beryllium in kornerupine. *Can. Mineral.* **47**, 303-313.

Cooper, M.A., Hawthorne, F.C., Grew, E.S. & Rossman, G.R. (2009b): The crystal chemistry of the kornerupine–prismatine series. II. The role of hydrogen. *Can. Mineral.* **47**, 263-274.

Finger, L.W. & Hazen, R.M. (1981): Refinement of the crystal structure of an iron-rich kornerupine. *Carnegie Inst. Wash., Year Book* **80**, 370-373.

Grew, E.S., Chernosky, J.V., Werding, G., Abraham, K., Marquez, N. & Hinthorne, J.R. (1990): Chemistry of kornerupine and associated minerals, a wet chemical, ion microprobe, and X-ray study emphasizing Li, Be, B and F contents. *J. Petrol.* **31**, 1025-1070.

Grew, E.S., Cooper, M.A. & Hawthorne, F.C. (1996): Prismatine: revalidation for boron-rich compositions in the kornerupine group. *Mineral. Mag.* **60**, 483-491.

Grew, E.S., Hiroi, Y., Motoyoshi, Y., Kondo, Y., Jayatileke, S.J.M. & Marquez, N. (1995): Iron-rich kornerupine in sheared pegmatite from the Wanni Complex, at Homogama, Sri Lanka. *Eur. J. Mineral.* **7**, 623-636.

GREW, E.S., REDHAMMER, G.J., AMTHAUER, G., COOPER, M.A., HAWTHORNE, F.C. & SCHMETZER, K. (1999): Iron in kornerupine: a ^{57}Fe Mössbauer spectroscopic study and comparison with single-crystal structure refinement. *Am. Mineral.* **84**, 536-549.

HAWTHORNE, F.C. (2002): The use of end-member charge-arrangements in defining new minerals and heterovalent substitutions in complex minerals. *Can. Mineral.* **40**, 699-710.

HAWTHORNE, F.C., COOPER, M.A., BOTTAZZI, P., OTTOLINI, L., ERCIT, T.S. & GREW, E.S. (1995): Micro-analysis of minerals for boron by SREF, SIMS, and EMPA: a comparative study. *Can. Mineral.* **33**, 389-397.

KLASKA, R. & GREW, E.S. (1991): The crystal structure of B-free kornerupine: conditions favoring the incorporation of variable amounts of B through $^{[4]}B \leftrightarrow {}^{[4]}Si$ substitution in kornerupine. *Am. Mineral.* **76**, 1824-1835.

MOORE, P.B. & ARAKI, T. (1979): Kornerupine: a detailed crystal-chemical study. *Neues Jahrb. Mineral., Abh.* **134**, 317-336.

MOORE, P.B. & BENNETT, J.M. (1968): Kornerupine: its crystal structure. *Science* **159**, 524-526.

MOORE, P.B., SEN GUPTA, P.K. & SCHLEMPER, E.O. (1989): Kornerupine: chemical crystallography, comparative crystallography, and its cation relation to olivine and to Ni_2In intermetallic. *Am. Mineral.* **74**, 642-655.

SHANNON, R.D. (1976): Revised effective ionic radii and systematic studies of interatomic distances in halides and chalcogenides. *Acta Crystallogr.* **A32**, 751-767.

Received March 16, 2006, revised manuscript accepted April 1, 2009.